Turbulent Flows

Stephen B. Pope
Cambridge University Press, 2000

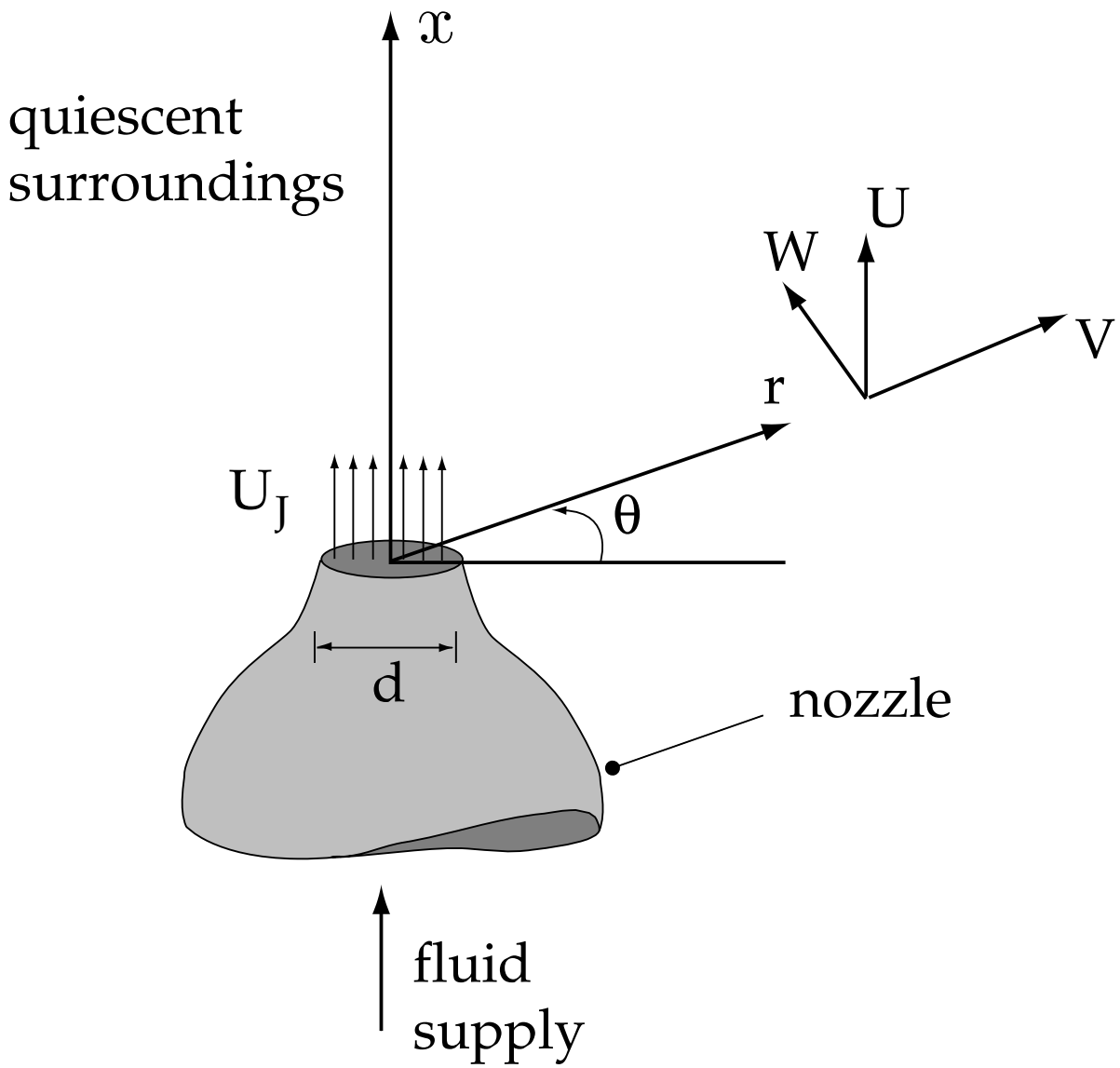

Figure 5.1: Sketch of a round jet experiment, showing the polar-cylindrical coordinate system employed.

Turbulent Flows

Stephen B. Pope
Cambridge University Press, 2000

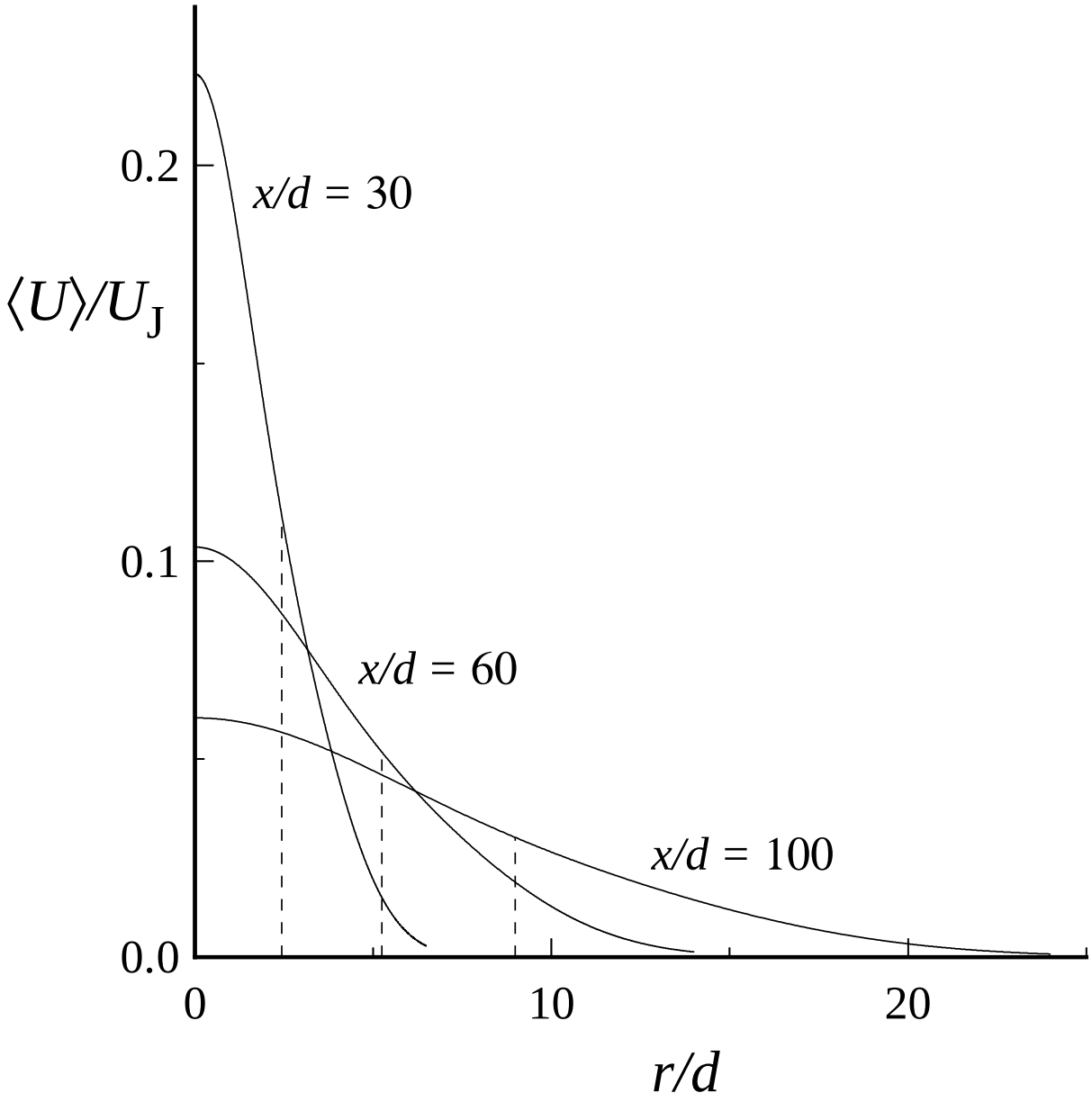

Figure 5.2: Radial profiles of mean axial velocity in a turbulent round jet, Re = 95, 500. The dashed lines indicate the half-width, $r_{\frac{1}{2}}(x)$, of the profiles. (Adapted from the data of Hussein et al. (1994).)

Turbulent Flows

Stephen B. Pope
Cambridge University Press, 2000

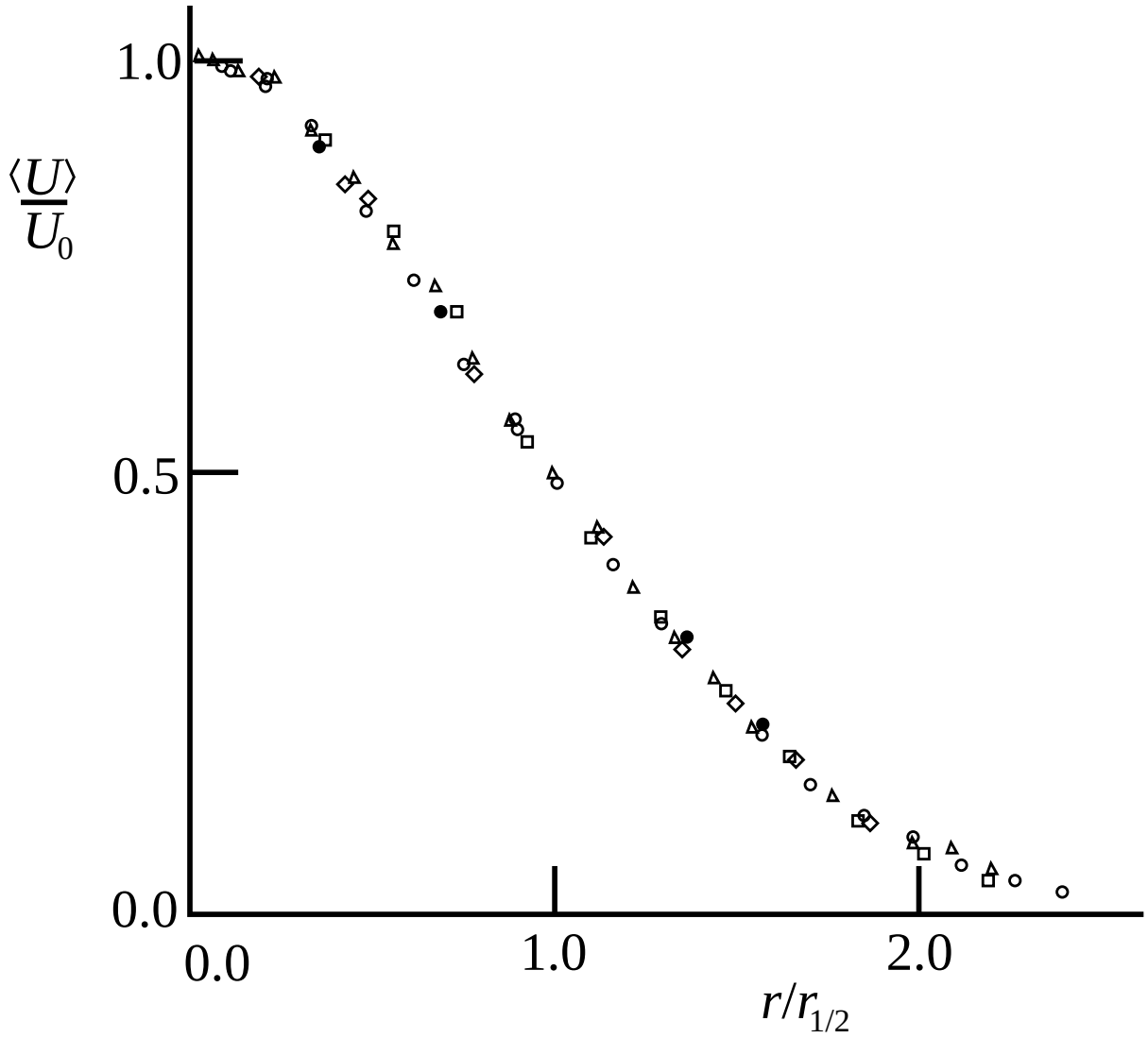

Figure 5.3: Mean axial velocity against radial distance in a turbulent round jet, Re $\approx 10^5$; measurements of Wygnanski and Fiedler (1969). Symbols: $\circ$, $x/d = 40$; $\triangle$, 50; $\square$, 60; $\Diamond$, 75; $\bullet$, 97.5.

Turbulent Flows

Stephen B. Pope
Cambridge University Press, 2000

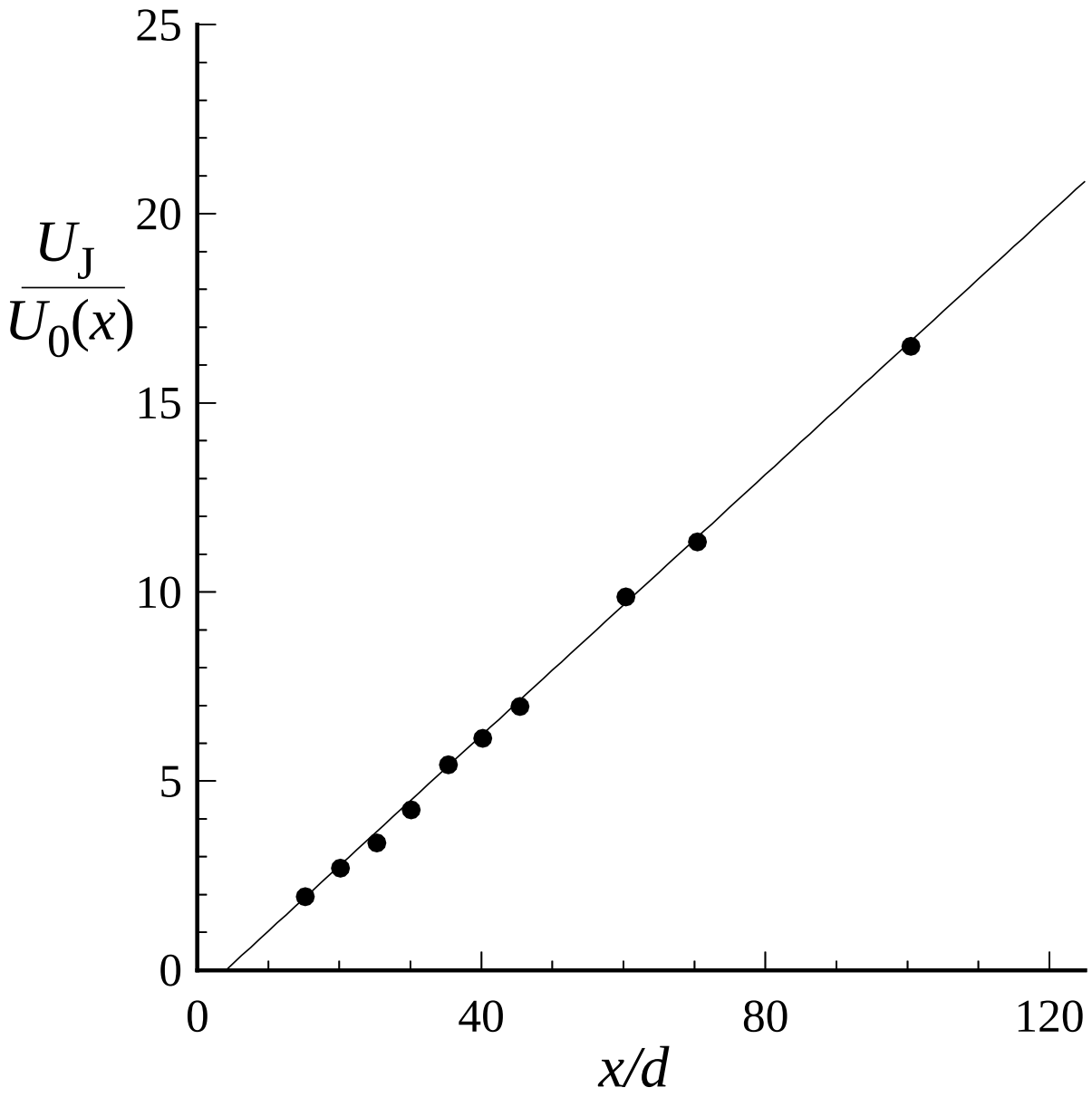

Figure 5.4: Centerline mean velocity variation with axial distance in a turbulent round jet, Re $= 95,500$: symbols, experimental data of Hussein et al. (1994), line—Eq. (5.6) with $x_0/d = 4, B = 5.8$.

Turbulent Flows

Stephen B. Pope

Cambridge University Press, 2000

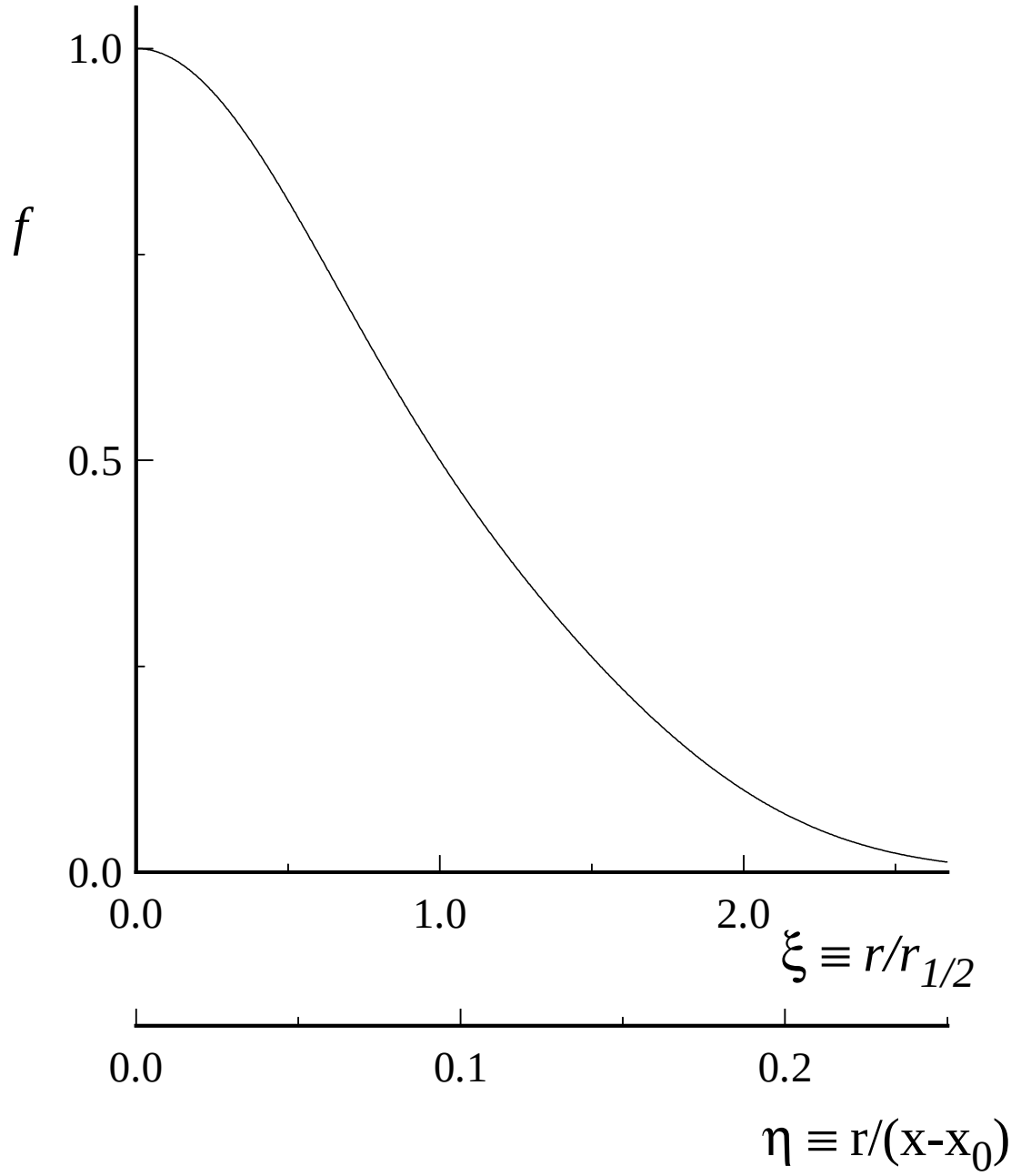

Figure 5.5: Self-similar profile of the mean axial velocity in the self-similar round jet. Curve fit to the LDA data of Hussein et al. (1994).

Turbulent Flows

Stephen B. Pope

Cambridge University Press, 2000

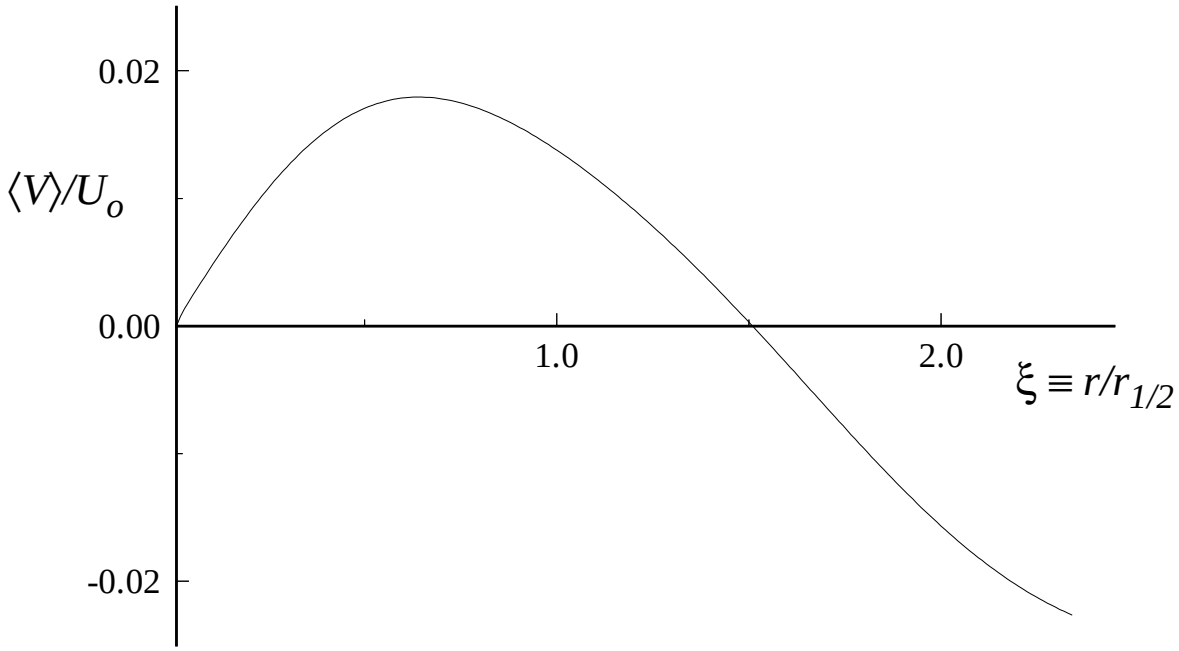

Figure 5.6: Mean lateral velocity in the self-similar round jet. From the LDA data of Hussein et al. (1994).

Turbulent Flows

Stephen B. Pope
Cambridge University Press, 2000

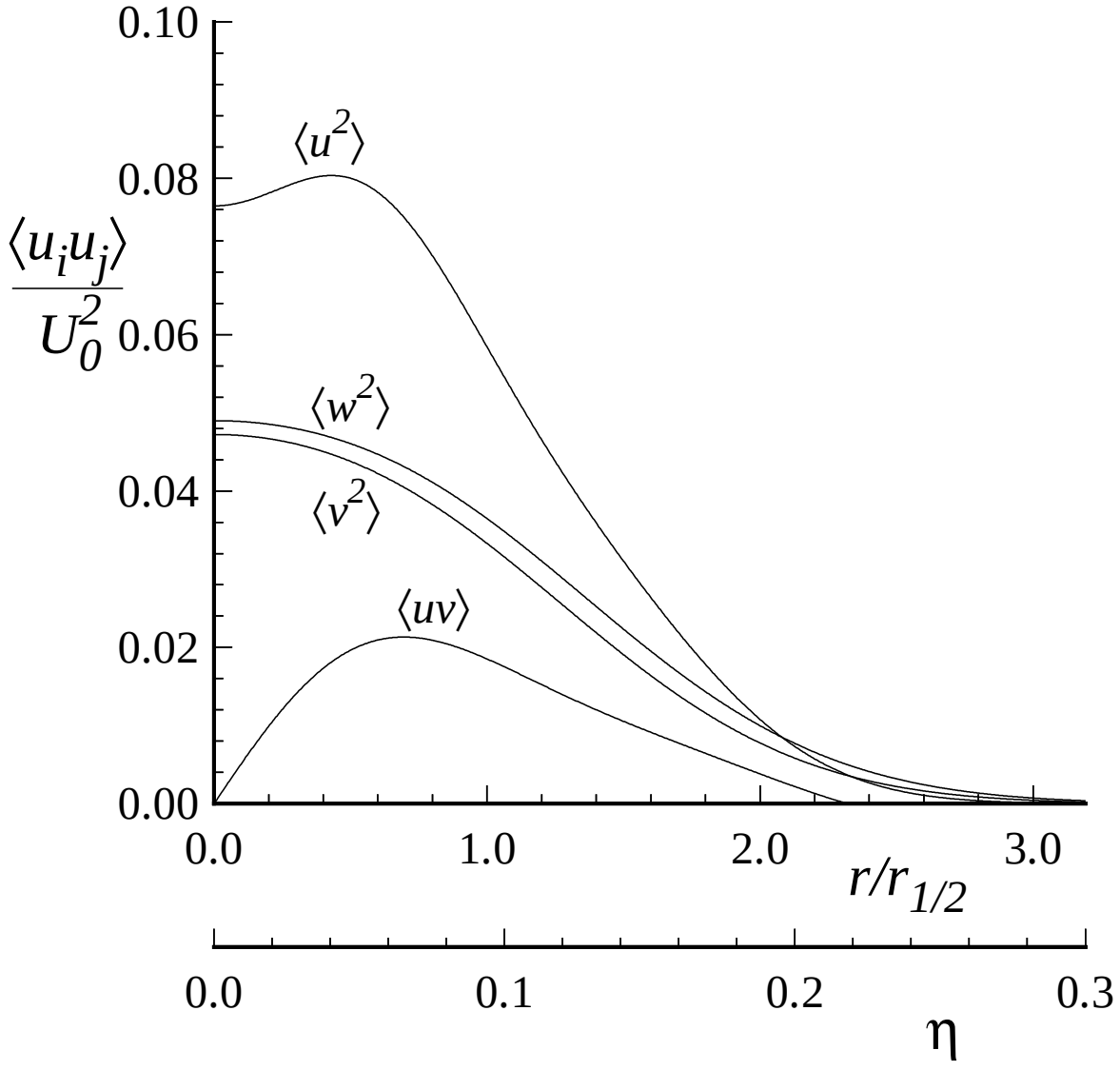

Figure 5.7: Profiles of Reynolds stresses in the self-similar round jet. Curve fit to the LDA data of Hussein et al. (1994).

Turbulent Flows

Stephen B. Pope
Cambridge University Press, 2000

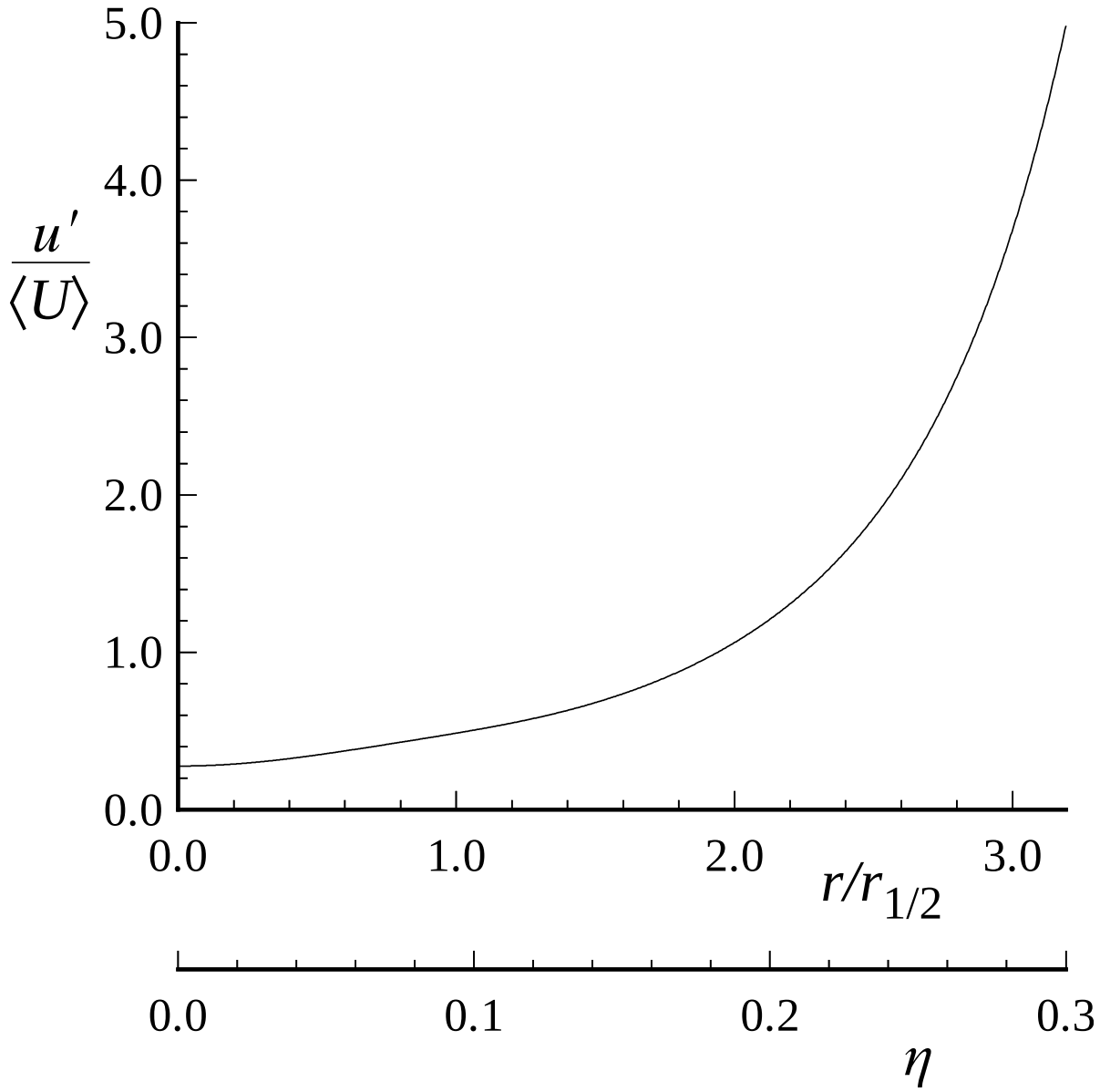

Figure 5.8: Profile of the local turbulence intensity—$\langle u^2 \rangle^{\frac{1}{2}} / \langle U \rangle$—in the self-similar round jet. From the curve fit to the experimental data of Hussein et al. (1994).

Turbulent Flows

Stephen B. Pope
Cambridge University Press, 2000

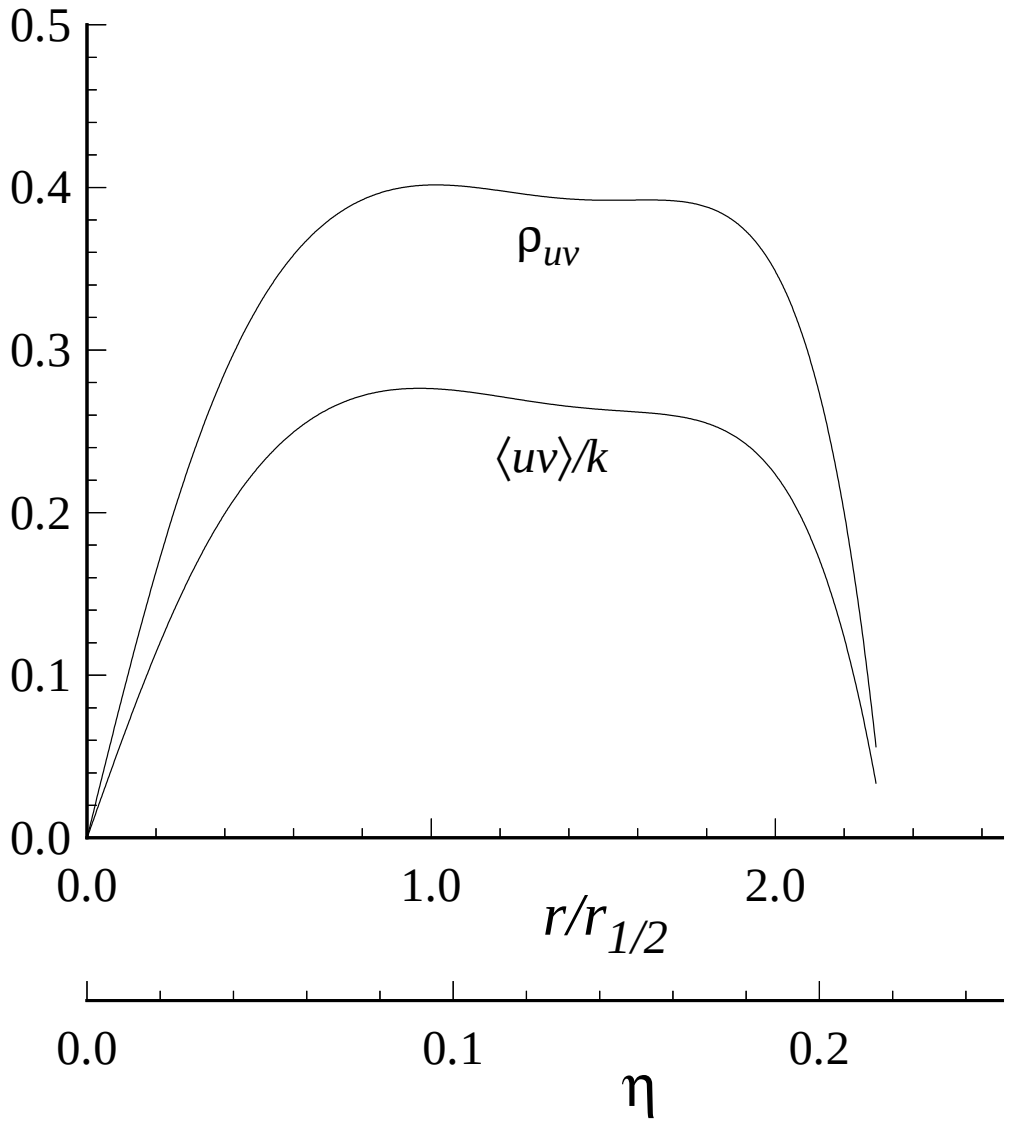

Figure 5.9: Profiles of $\langle uv \rangle / k$ and the u-v correlation coefficient ρ_{uv} in the self-similar round jet. From the curve fit to the experimental data of Hussein et al. (1994).

Turbulent Flows

Stephen B. Pope
Cambridge University Press, 2000

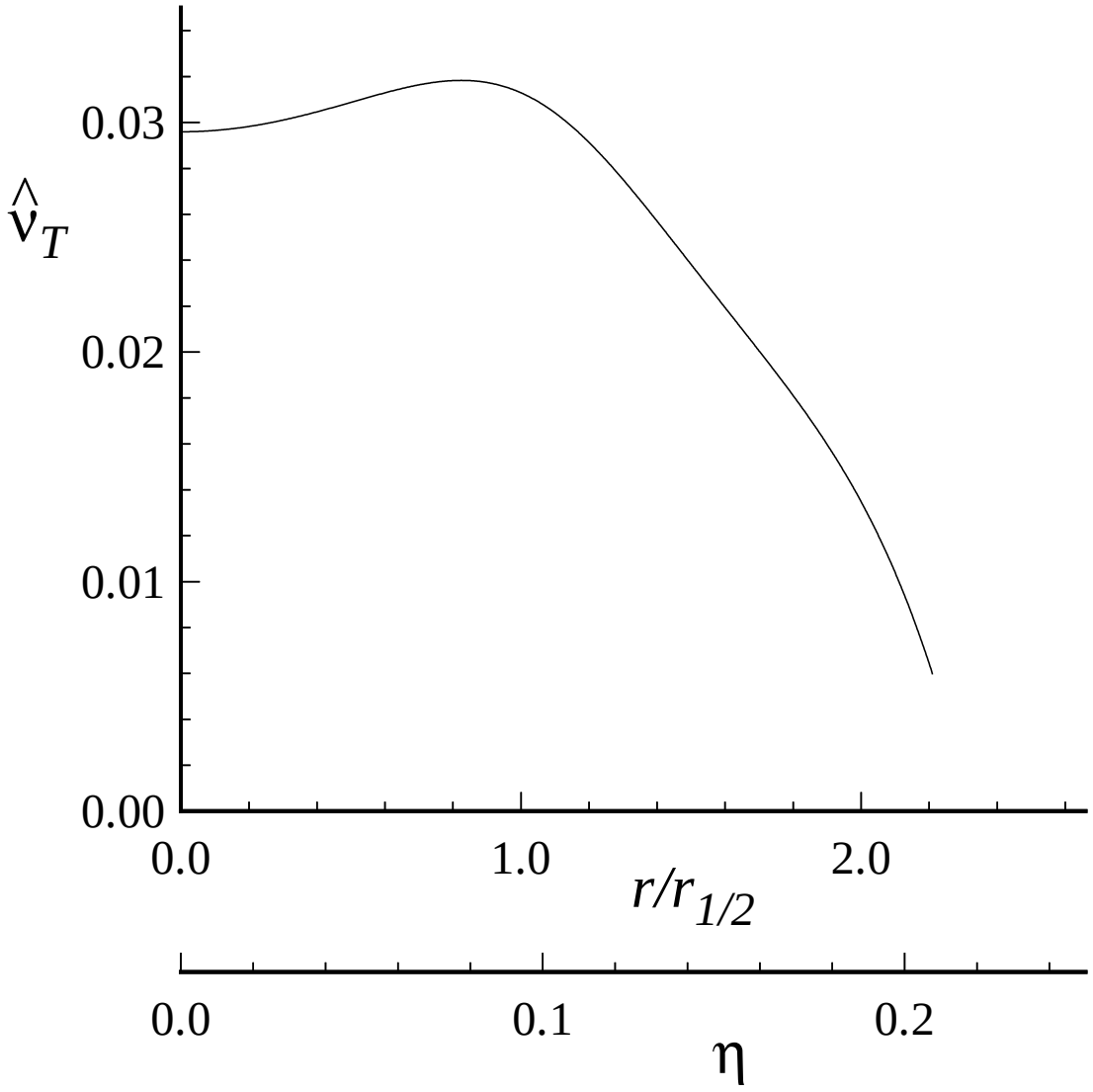

Figure 5.10: Normalized turbulent diffusivity $\hat{\nu}_T$ (Eq. (5.34)) in the self-similar round jet. From the curve fit to the experimental data of Hussein et al. (1994).

Turbulent Flows

Stephen B. Pope
Cambridge University Press, 2000

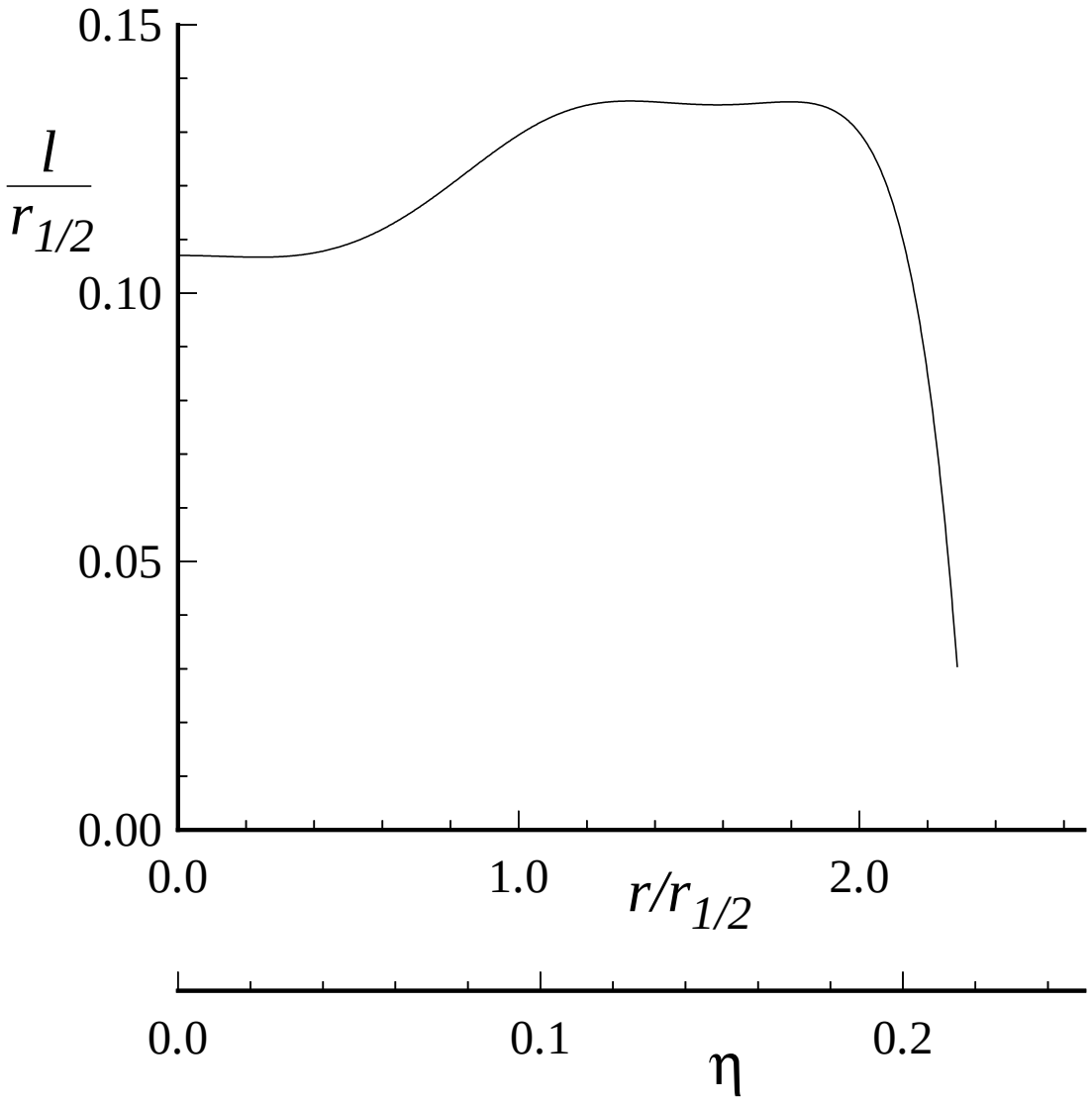

Figure 5.11: Profile of the lengthscale defined by (Eq. (5.35)) in the self-similar round jet. From the curve fit to the experimental data of Hussein et al. (1994).

Turbulent Flows

Stephen B. Pope
Cambridge University Press, 2000

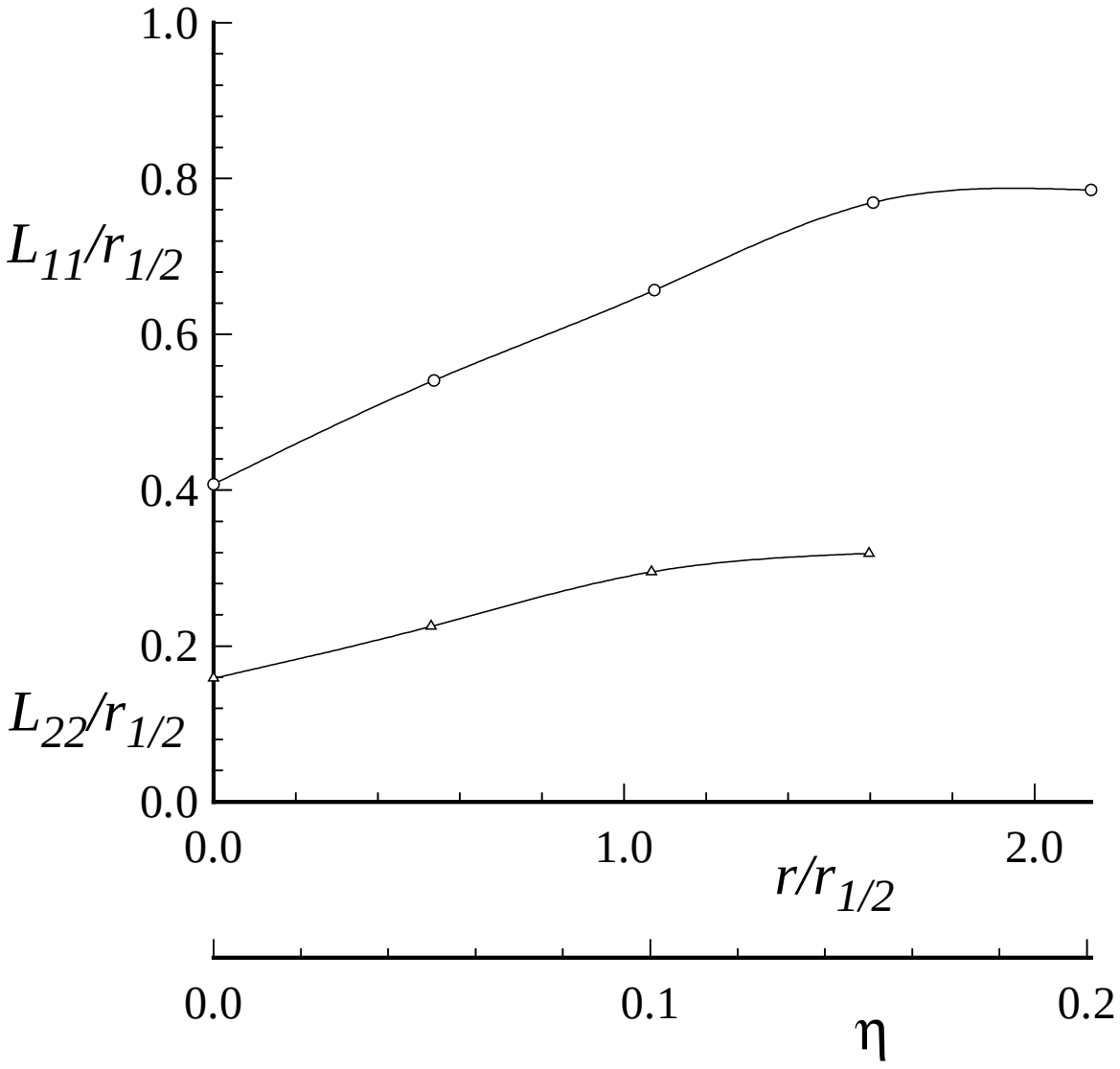

Figure 5.12: Self-similar profiles of the integral lengthscales in the turbulent round jet. From Wygnanski and Fiedler (1969).

Turbulent Flows

Stephen B. Pope
Cambridge University Press, 2000

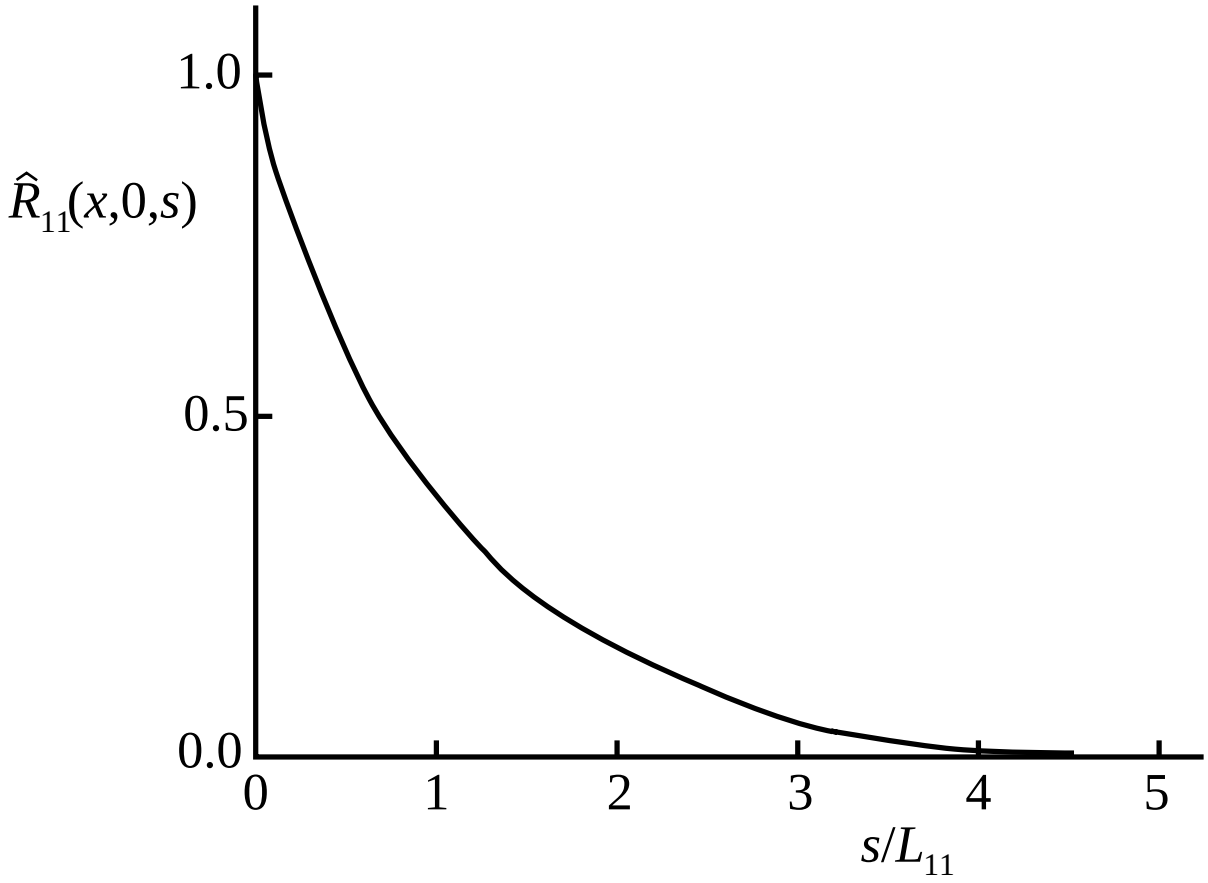

Figure 5.13: Longitudinal autocorrelation of the axial velocity in the self-similar round jet. From Wygnanski and Fiedler (1969).

CHAPTER 5: FREE SHEAR FLOWS

Turbulent Flows

Stephen B. Pope
Cambridge University Press, 2000

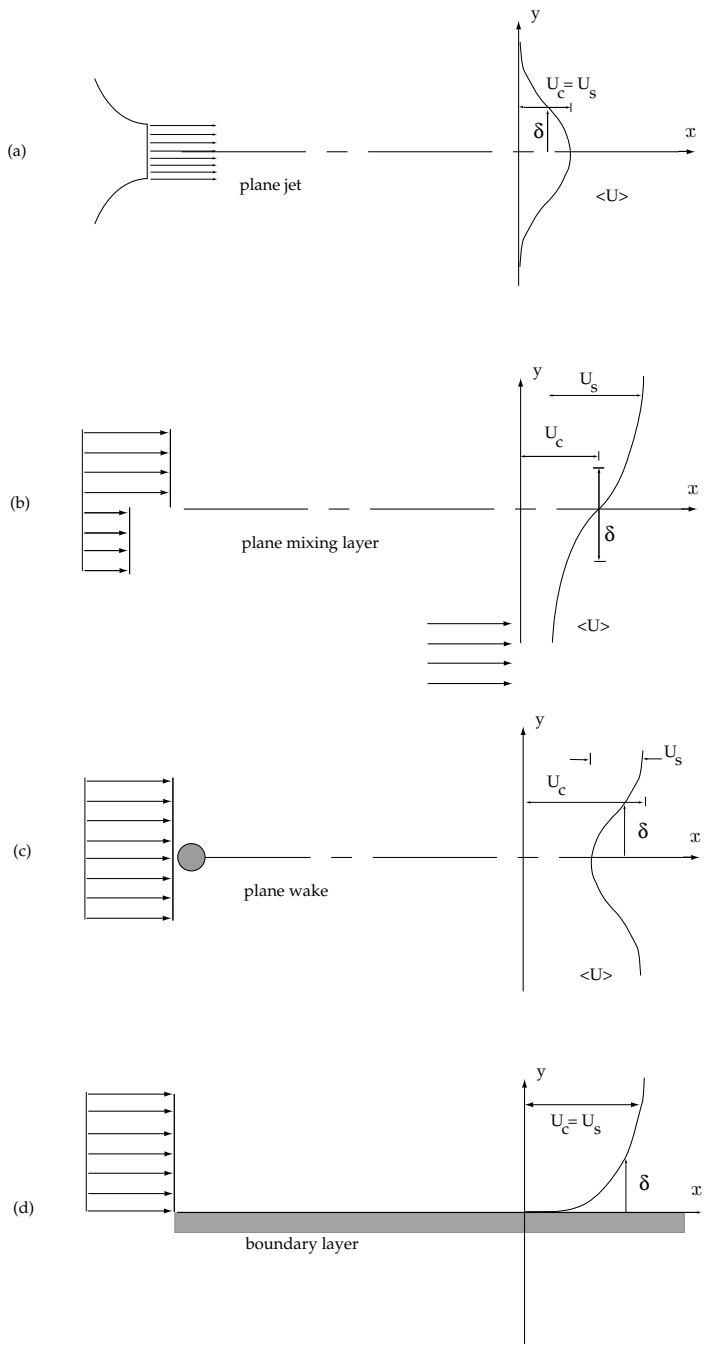

Figure 5.14: Sketch of plane two-dimensional shear flows showing the characteristic flow width $\delta(x)$, the characteristic convective velocity U_c, and the characteristic velocity difference U_s.

Turbulent Flows

Stephen B. Pope
Cambridge University Press, 2000

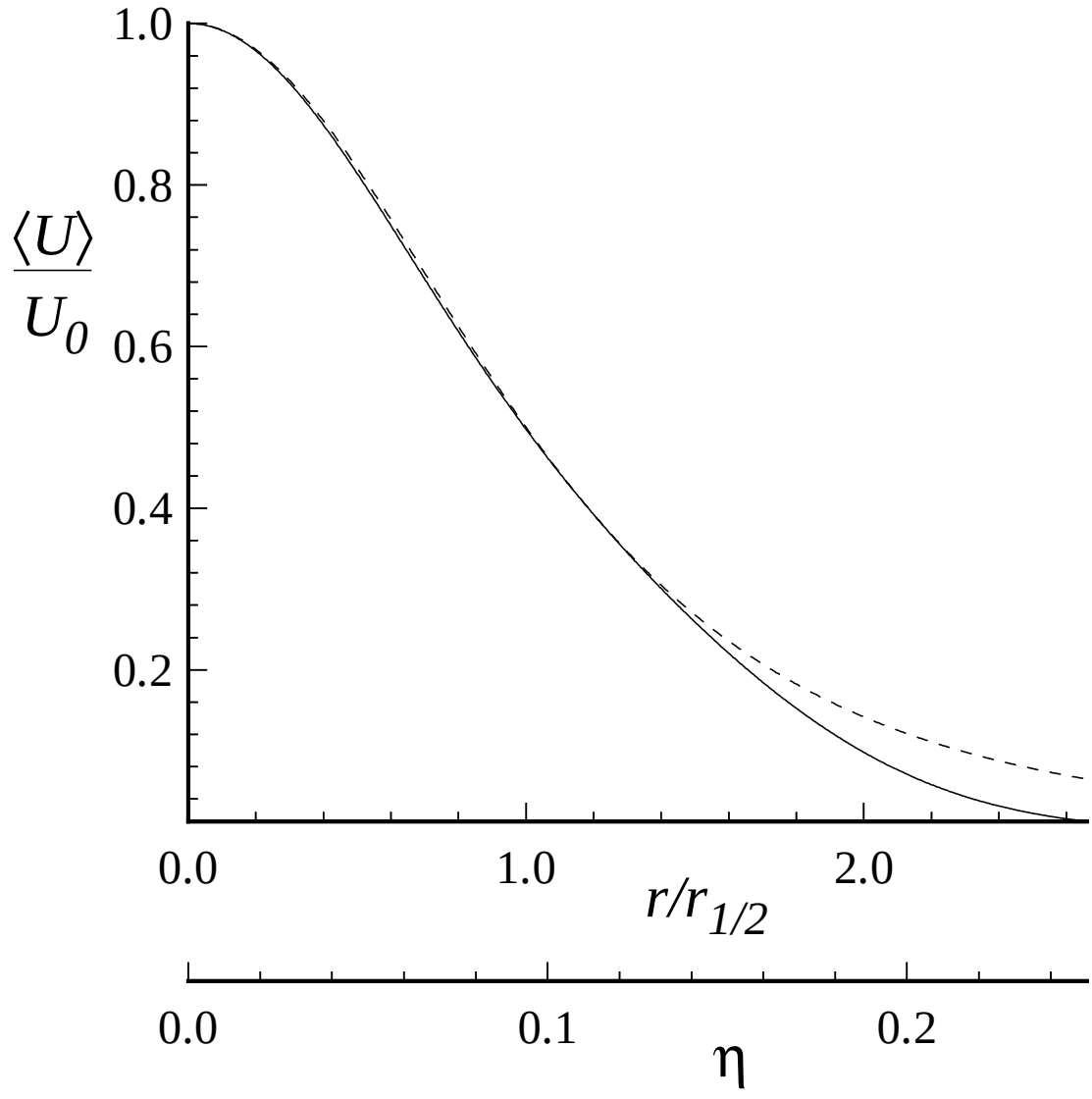

Figure 5.15: Mean velocity profile in the self-similar round jet: solid line, curve fit to the experimental data of Hussein et al. (1994); dashed line, uniform turbulent viscosity solution (Eq. 5.82).

Turbulent Flows

Stephen B. Pope
Cambridge University Press, 2000

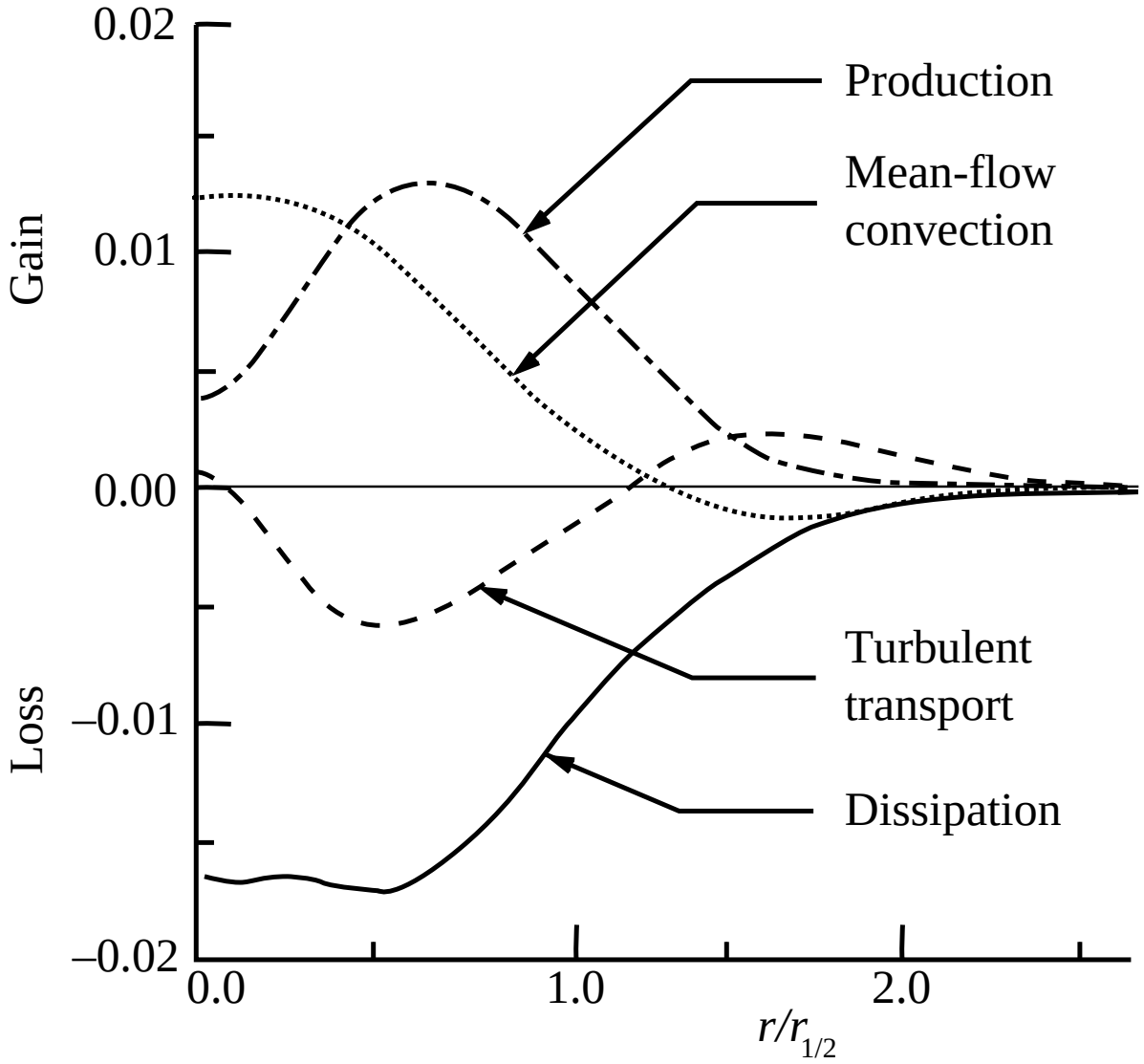

Figure 5.16: Turbulent kinetic energy budget in the self-similar round jet. Quantities are normalized by U_0 and $r_{\frac{1}{2}}$. (From Panchapakesan and Lumley (1993a).)

Turbulent Flows

Stephen B. Pope
Cambridge University Press, 2000

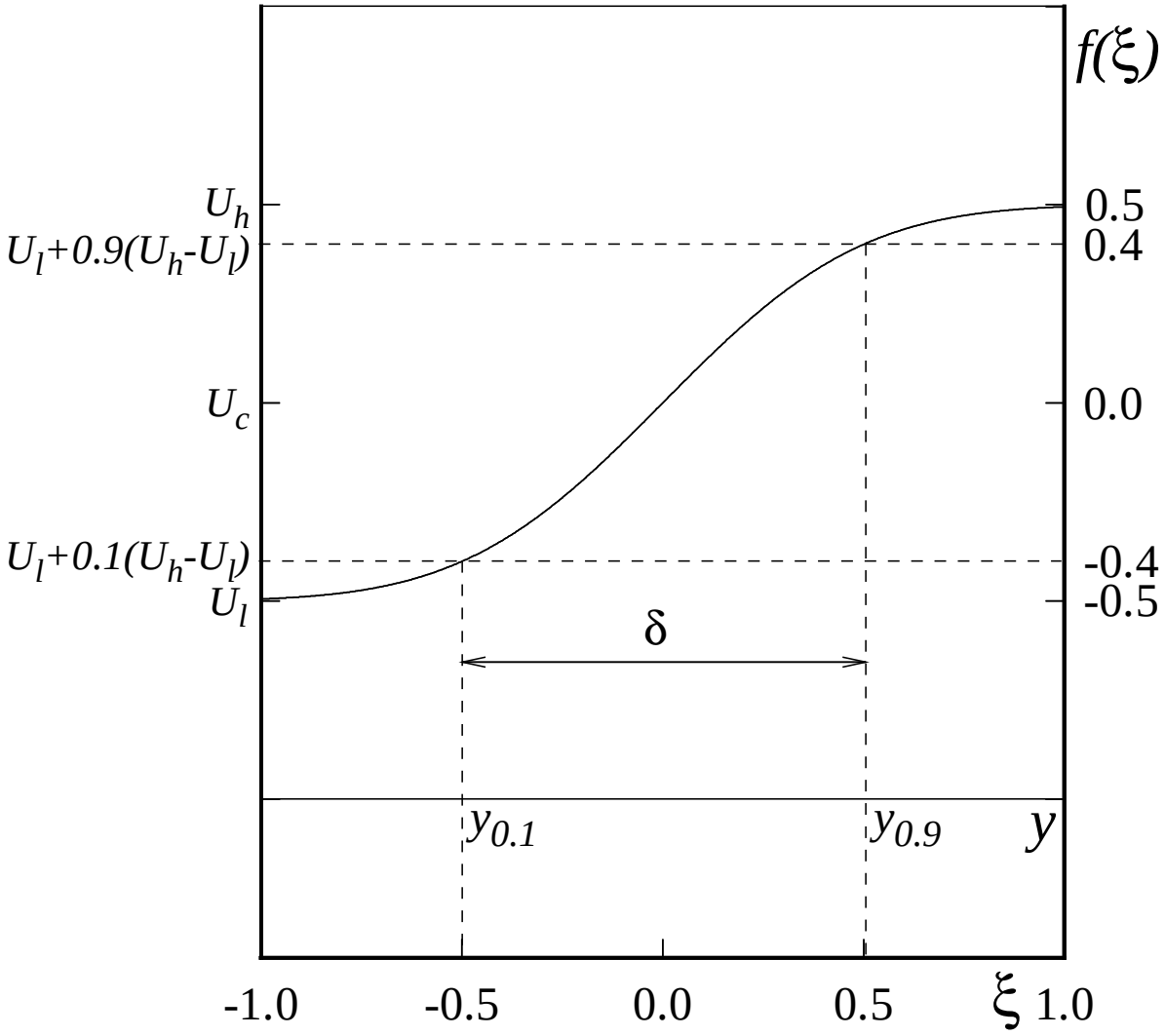

Figure 5.21: Sketch of the mean velocity $\langle U \rangle$ against y, and of the scaled mean velocity profile $f(\xi)$, showing the definitions of $y_{0.1}$, $y_{0.9}$ and δ.

Turbulent Flows

Stephen B. Pope
Cambridge University Press, 2000

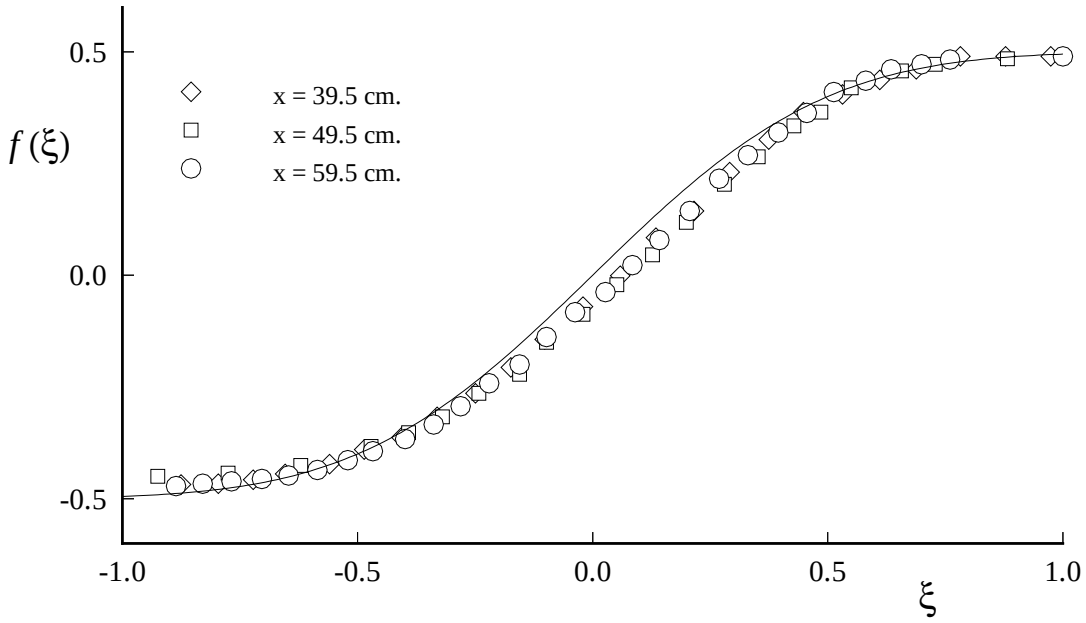

Figure 5.22: Scaled velocity profiles in a plane mixing layer. Symbols, experimental data of Champagne et al. (1976); line, error-function profile (Eq. (5.224)) shown for reference.

Turbulent Flows

Stephen B. Pope
Cambridge University Press, 2000

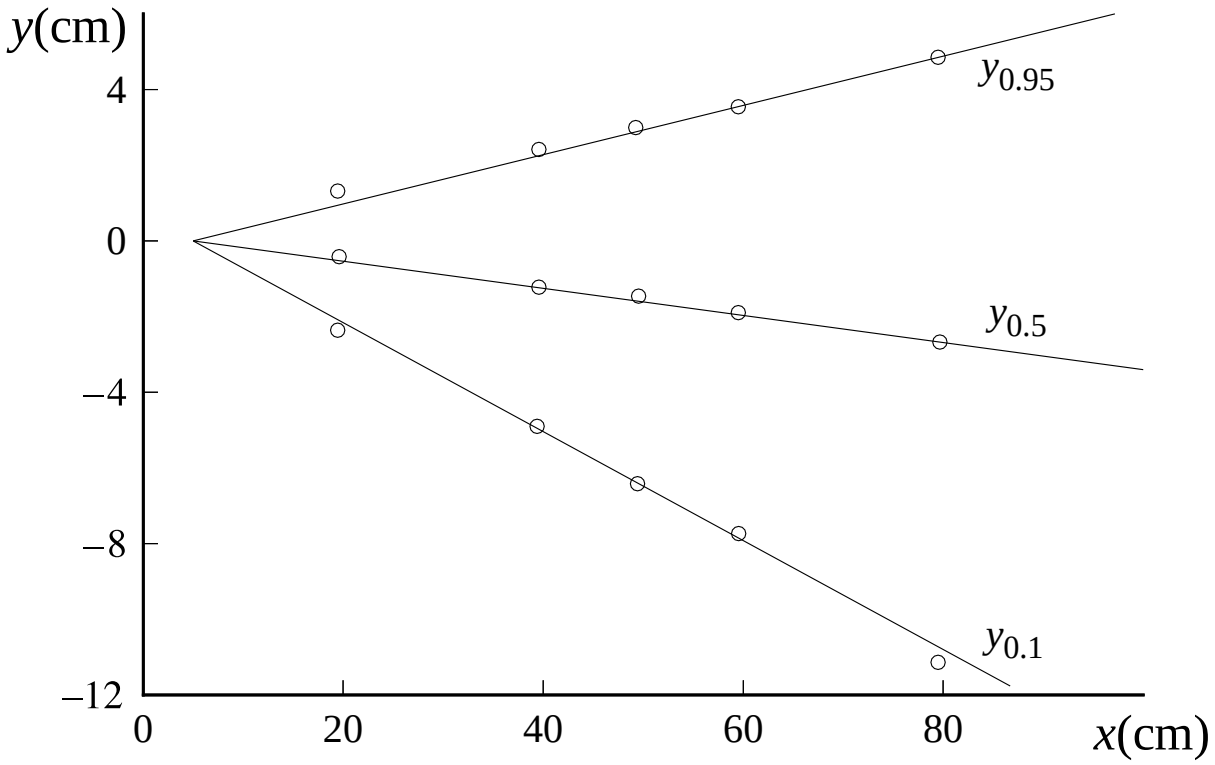

Figure 5.23: Axial variation of $y_{0.1}, y_{0.5}$ and $y_{0.95}$ in the plane mixing layer, showing the linear spreading. Experimental data of Champagne et al. (1976).

Turbulent Flows

Stephen B. Pope

Cambridge University Press, 2000

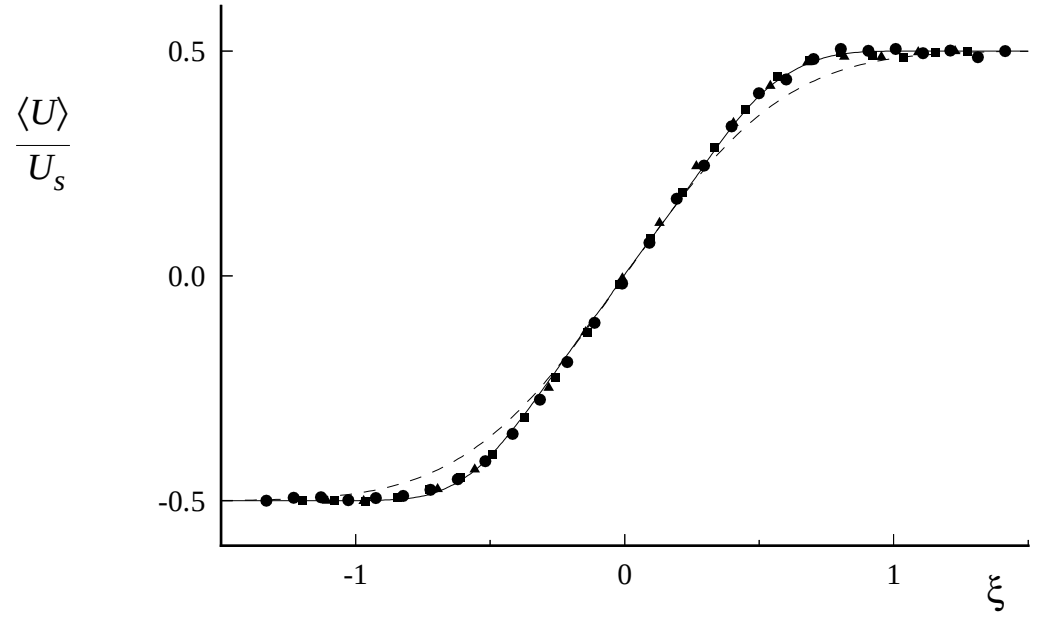

Figure 5.24: Scaled mean velocity profile in self-similar plane mixing layers. Symbols, experiment of Bell and Mehta (1990) ($U_\ell/U_h = 0.6$); solid line, DNS data for the temporal mixing layer (Rogers and Moser 1994); dashed line error-function profile with width chosen to match data in the center of the layer.

Turbulent Flows

Stephen B. Pope
Cambridge University Press, 2000

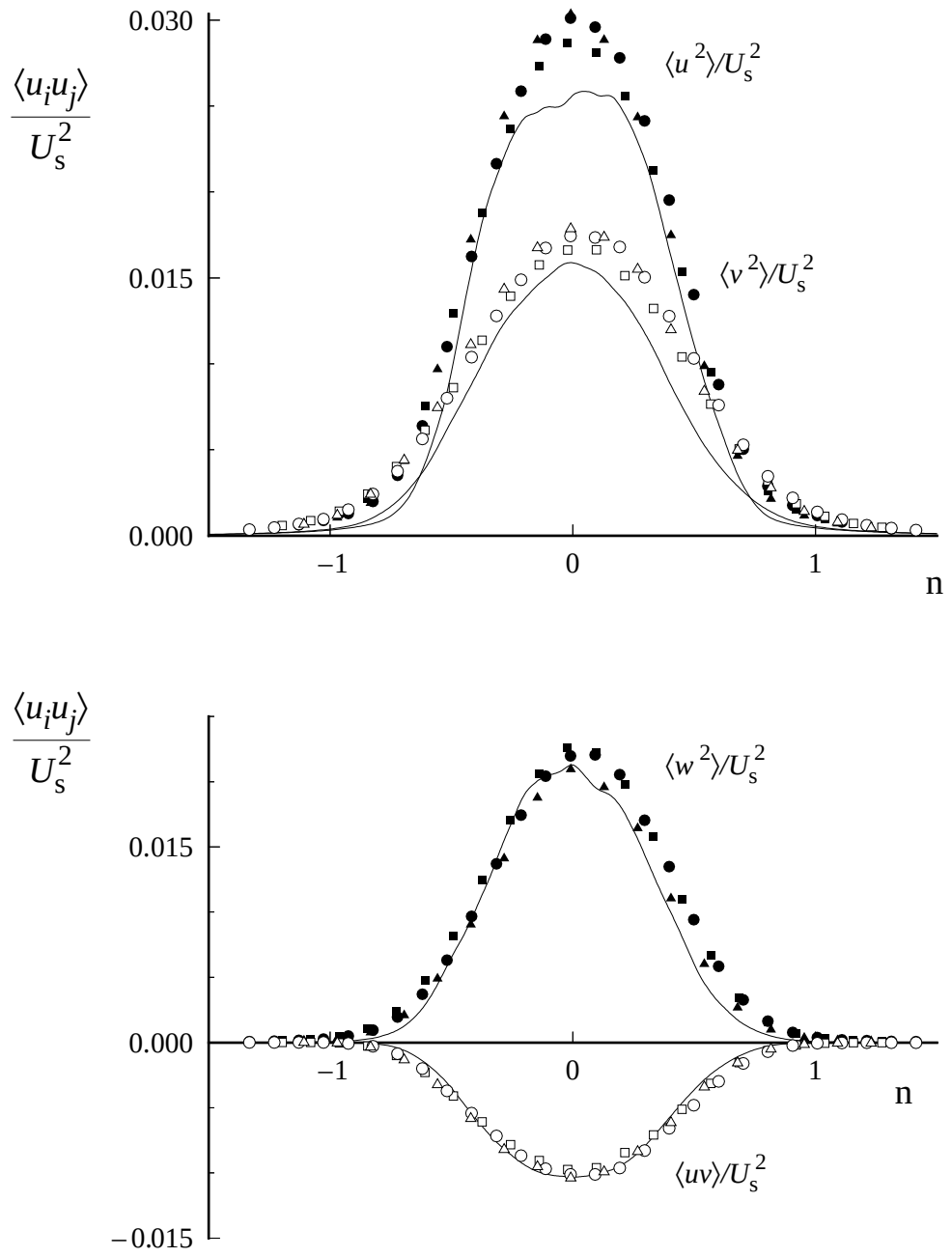

Figure 5.25: Scaled Reynolds stress profiles in self-similar plane mixing layers. Symbols, experiment of Bell and Mehta (1990) ($U_\ell/U_h = 0.6$); solid line, DNS data for the temporal mixing layer (Rogers and Moser 1994).

Turbulent Flows

Stephen B. Pope
Cambridge University Press, 2000

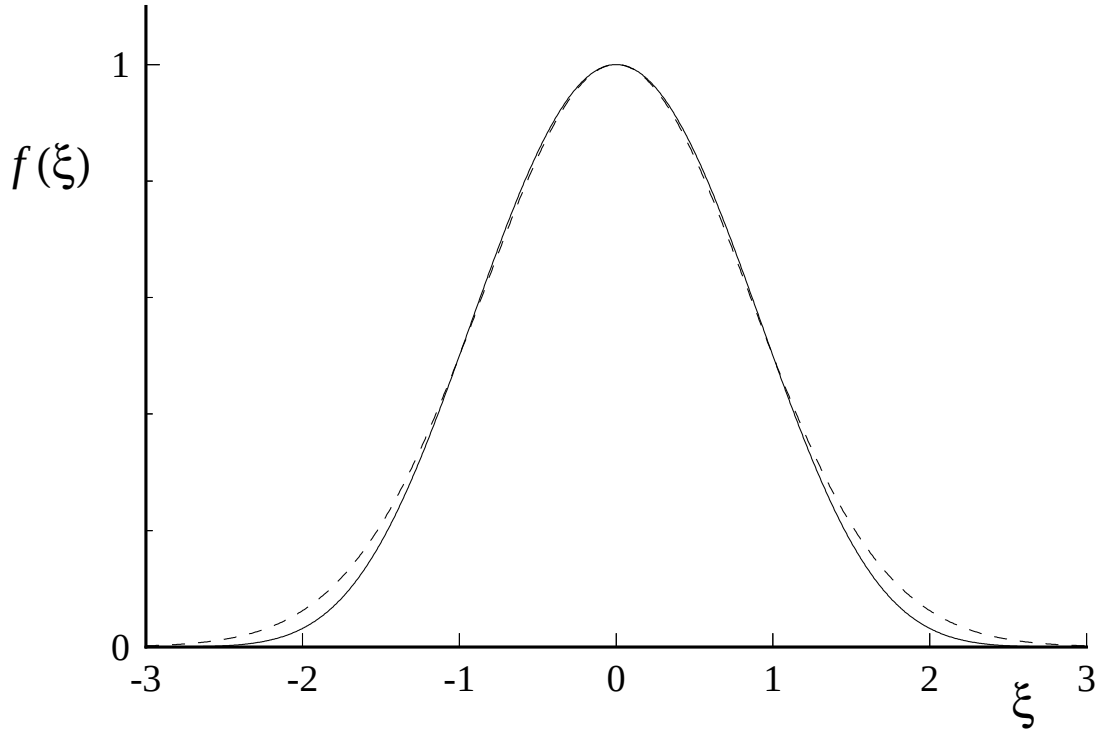

Figure 5.26: Normalized velocity defect profile in the self-similar plane wake. Solid line, from experimental data of Wygnanski et al. (1986); dashed line, constant-turbulent-viscosity solution, Eq. (5.240).

Turbulent Flows

Stephen B. Pope
Cambridge University Press, 2000

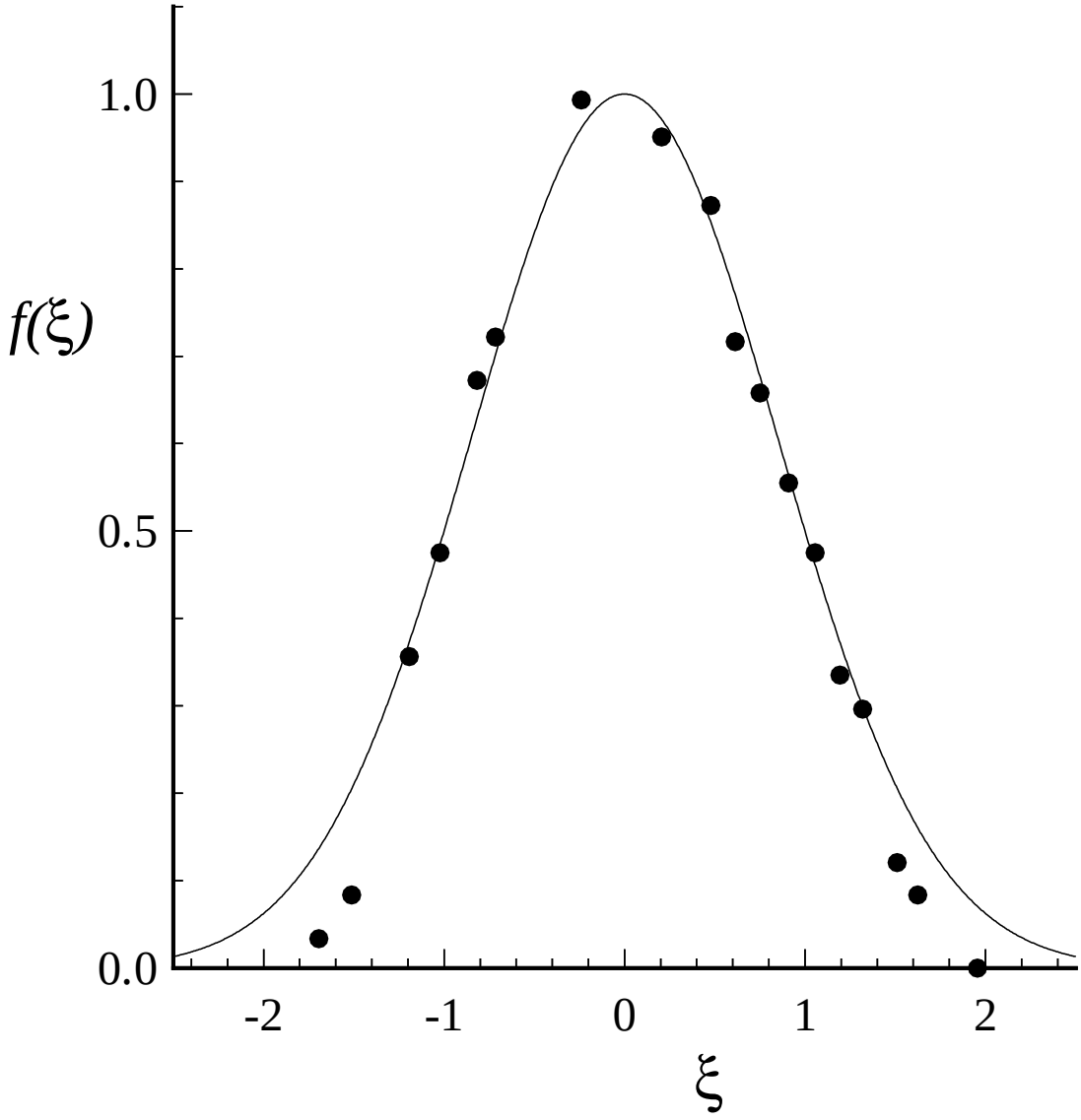

Figure 5.27: Mean velocity deficit profiles in a self-similar axisymmetric wake. Symbols, experimental data of Uberoi and Freymuth (1970); line, constant-turbulent-viscosity solution $f(\xi) = \exp(-\xi^2 \ln 2)$

Turbulent Flows

Stephen B. Pope

Cambridge University Press, 2000

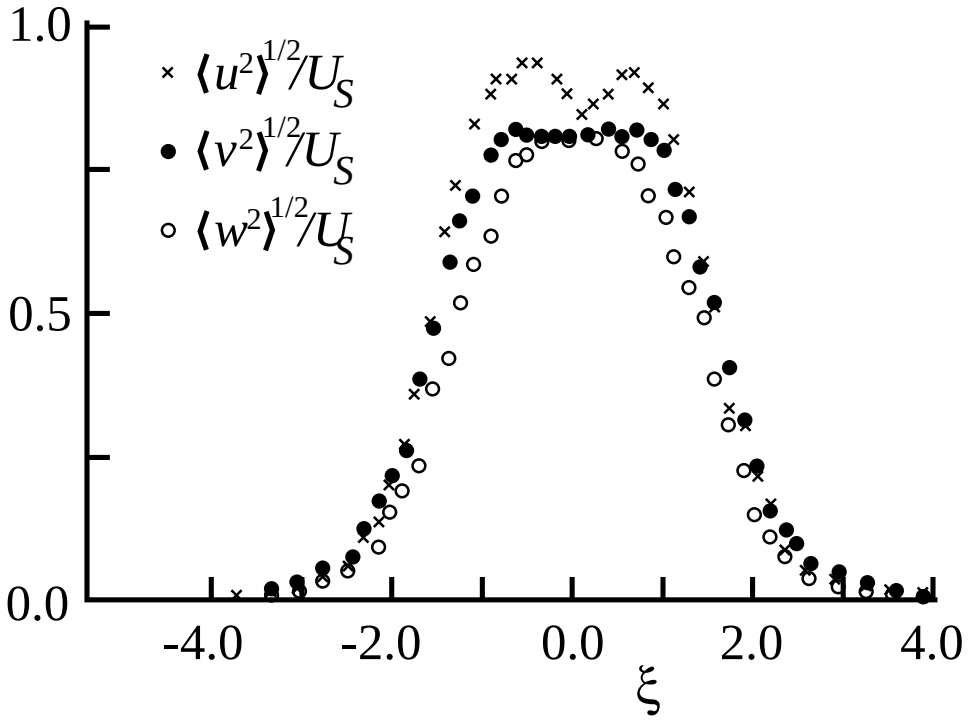

Figure 5.28: R.m.s. velocity profiles in a self-similar axisymmetric wake. Experimental data of Uberoi and Freymuth (1970).

Turbulent Flows

Stephen B. Pope
Cambridge University Press, 2000

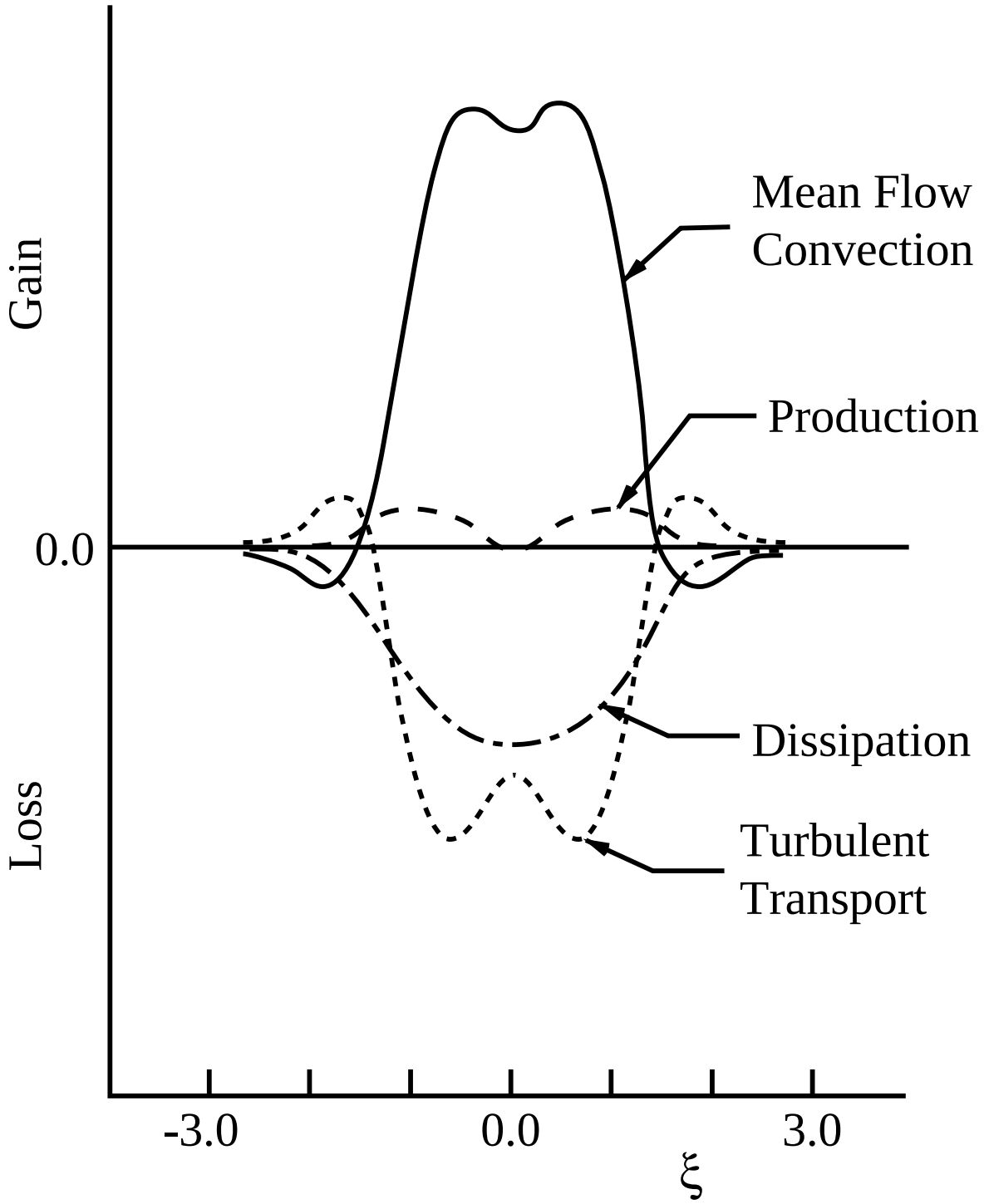

Figure 5.29: Turbulent kinetic energy budget in a self-similar axisymmetric wake. Experimental data of Uberoi and Freymuth (1970).

Turbulent Flows

Stephen B. Pope
Cambridge University Press, 2000

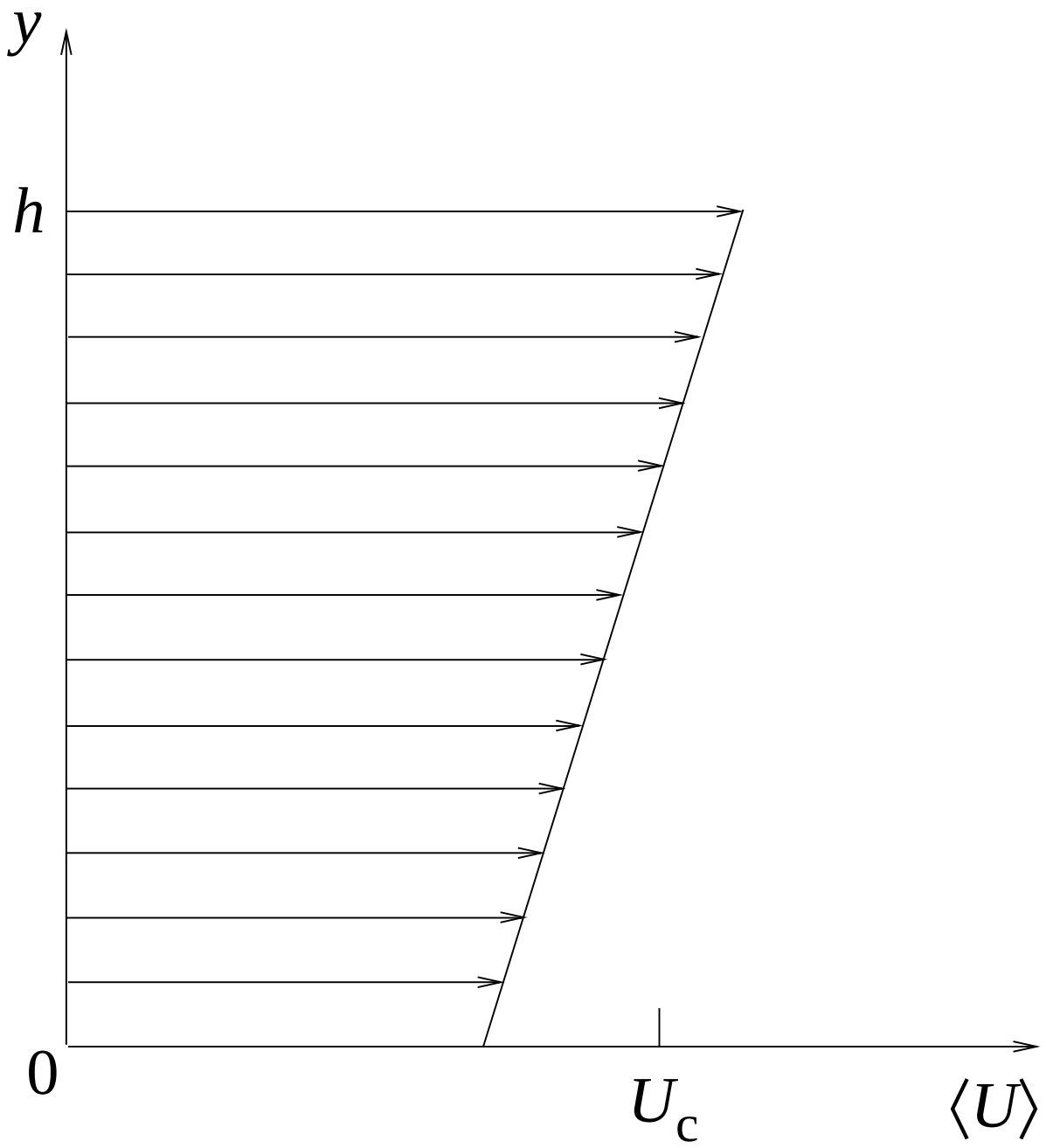

Figure 5.30: Sketch of the mean velocity profile in homogeneous shear flow.

Turbulent Flows

Stephen B. Pope
Cambridge University Press, 2000

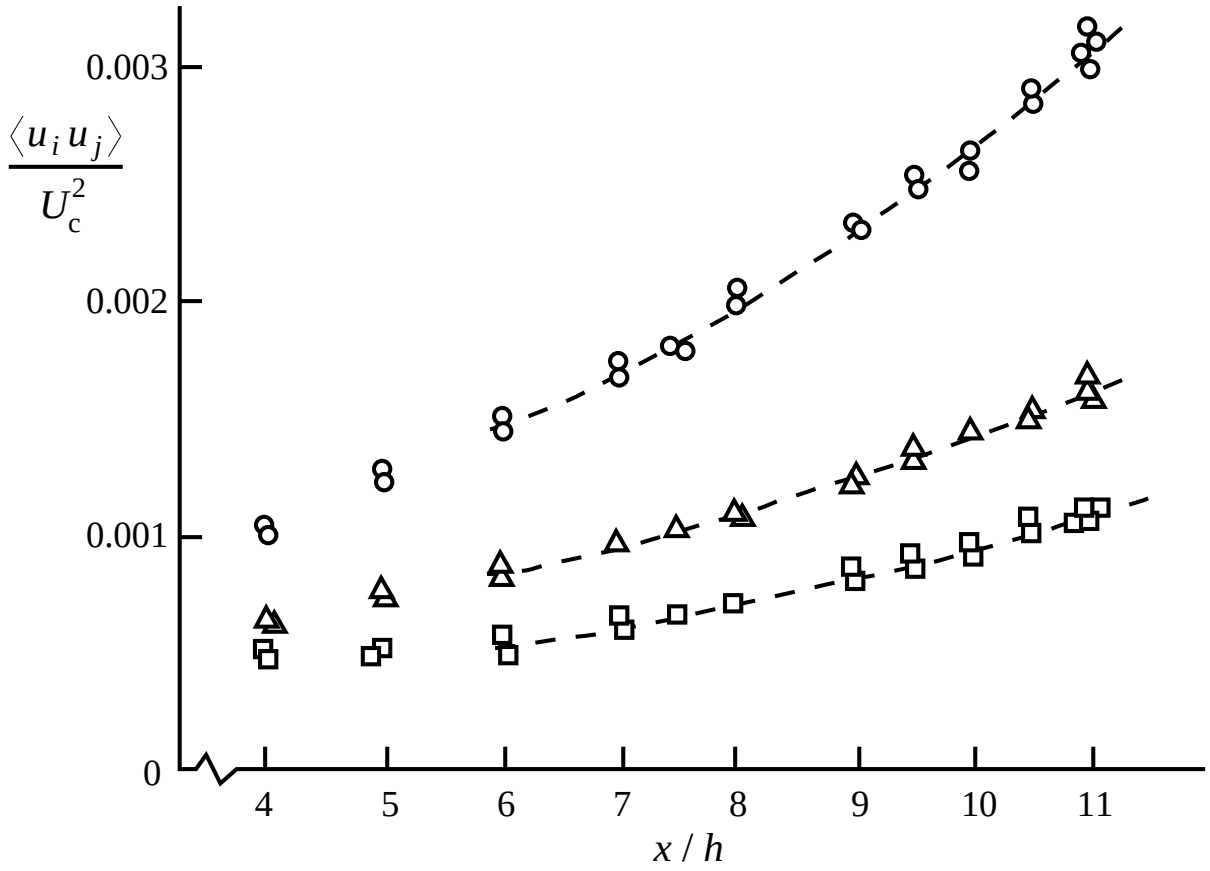

Figure 5.31: Reynolds stresses against axial distance in the homogeneous shear flow experiment of Tavoularis and Corrsin (1981): ◯, $\langle u^2 \rangle$; □, $\langle v^2 \rangle$; △, $\langle w^2 \rangle$.

Turbulent Flows

Stephen B. Pope
Cambridge University Press, 2000

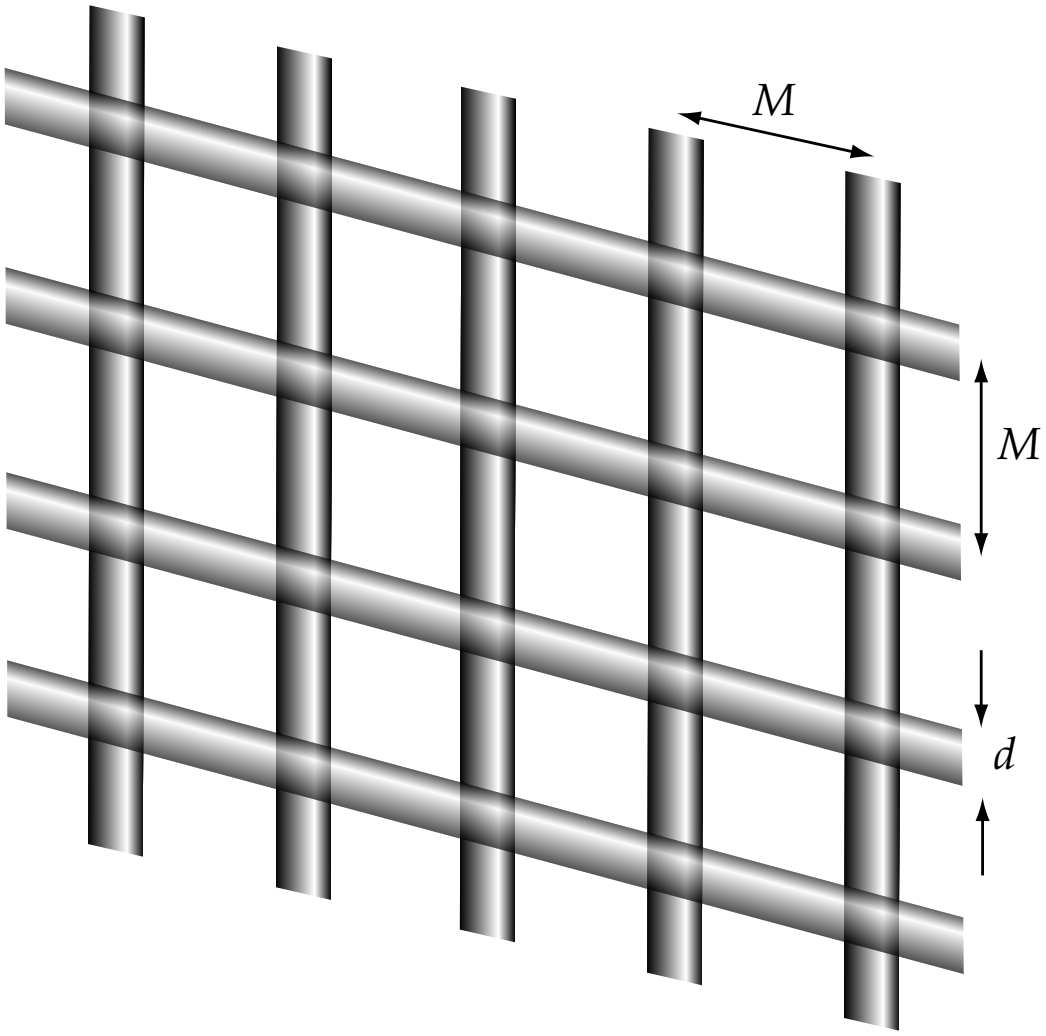

Figure 5.32: Sketch of a turbulence generating grid composed of bars of diameter d, with mesh spacing M.

Turbulent Flows

Stephen B. Pope
Cambridge University Press, 2000

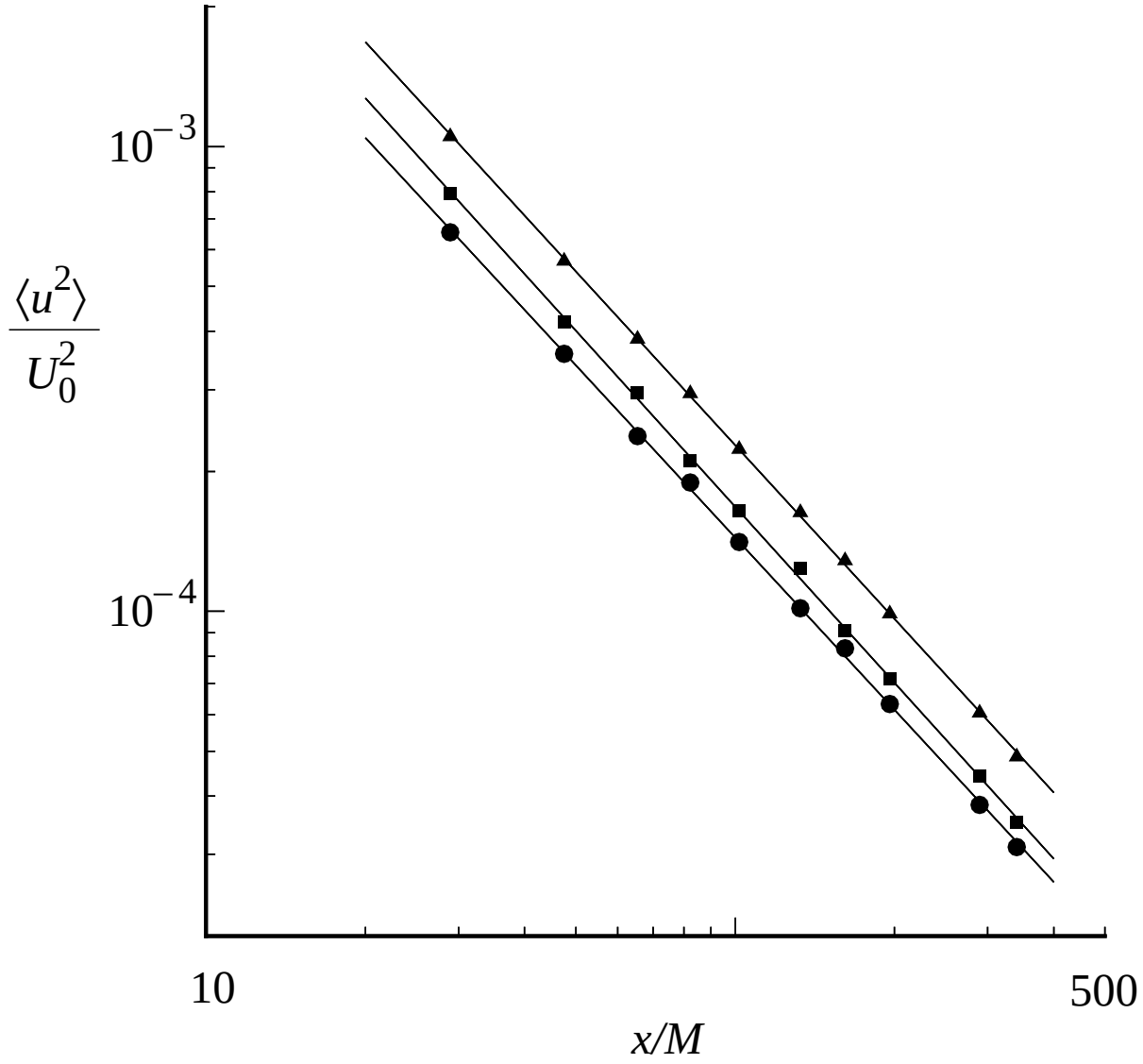

Figure 5.33: Decay of Reynolds stresses in grid turbulence: squares $\langle u^2 \rangle / U_0^2$; circles $\langle v^2 \rangle / U_0^2$; triangles k/U_0^2 ; lines, proportional to $(x/M)^{-1.3}$. (From Comte-Bellot and Corrsin (1966).)

Turbulent Flows

Stephen B. Pope
Cambridge University Press, 2000

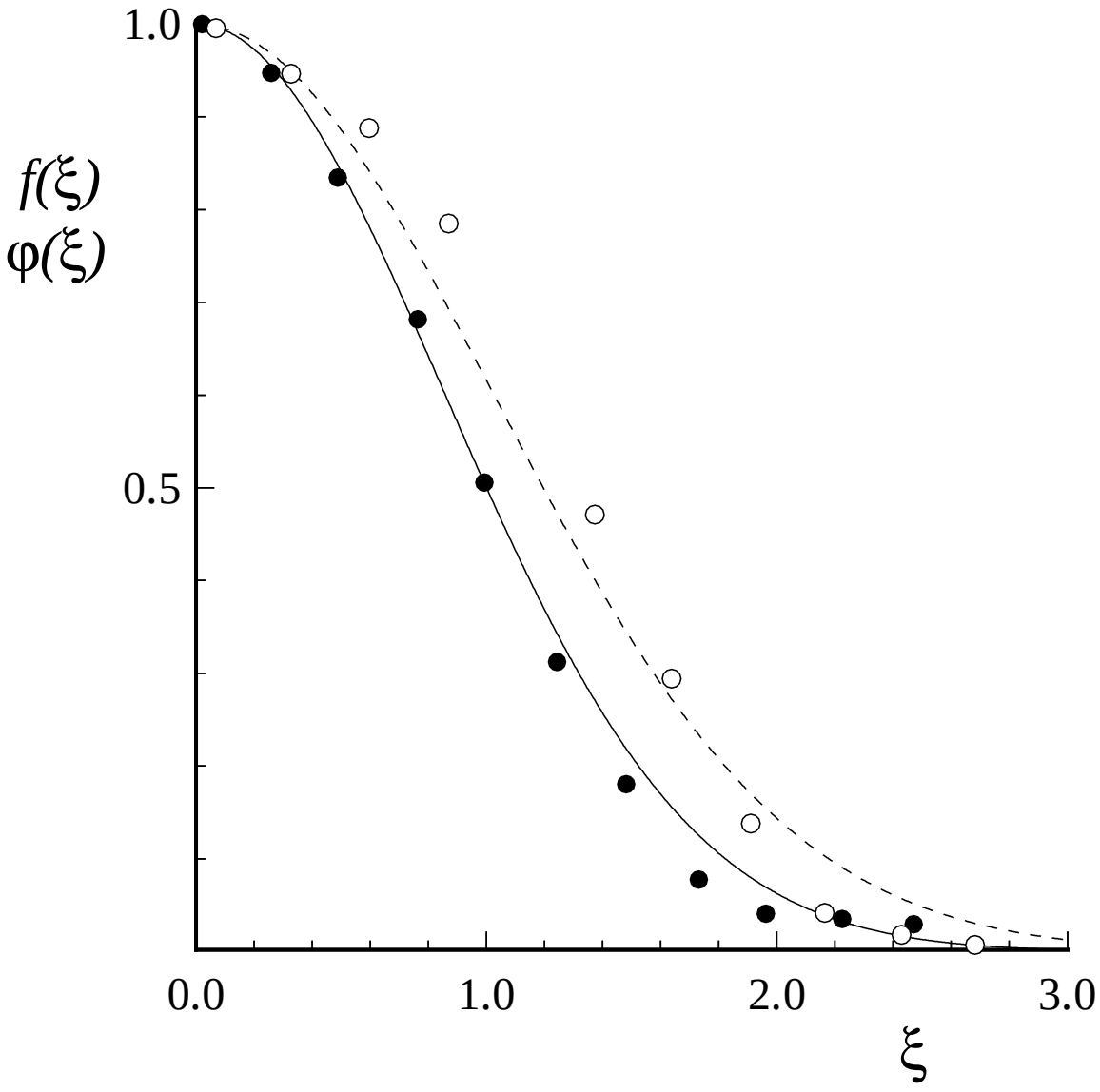

Figure 5.34: Normalized mean velocity deficit $f(\xi)$ and scalar, $\varphi(\xi) = \langle\phi\rangle/\langle\phi\rangle_{y=0}$ in the self-similar plane wake. Symbols (solid f, open φ) experimental data of Fabris (1979); solid line, $f(\xi) = \exp(-\xi^2 \ln 2)$; dashed line, $\varphi(\xi) = \exp(-\xi^2 \sigma_T \ln 2)$ with $\sigma_T = 0.7$.

Turbulent Flows

Stephen B. Pope
Cambridge University Press, 2000

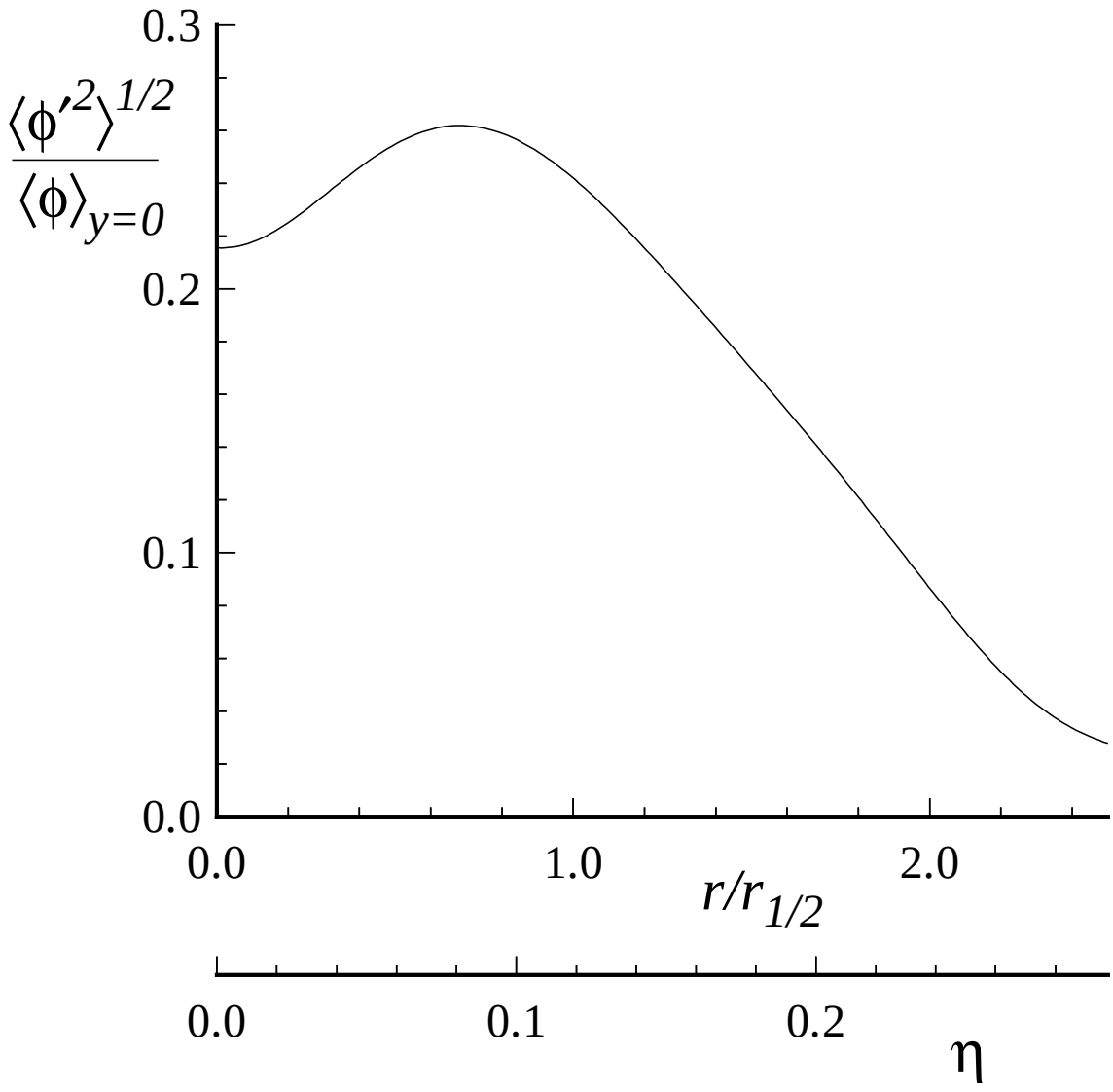

Figure 5.35: Normalized r.m.s. scalar fluctuations in a round jet. From the experimental data of Panchapakesan and Lumley (1993b).

Turbulent Flows

Stephen B. Pope
Cambridge University Press, 2000

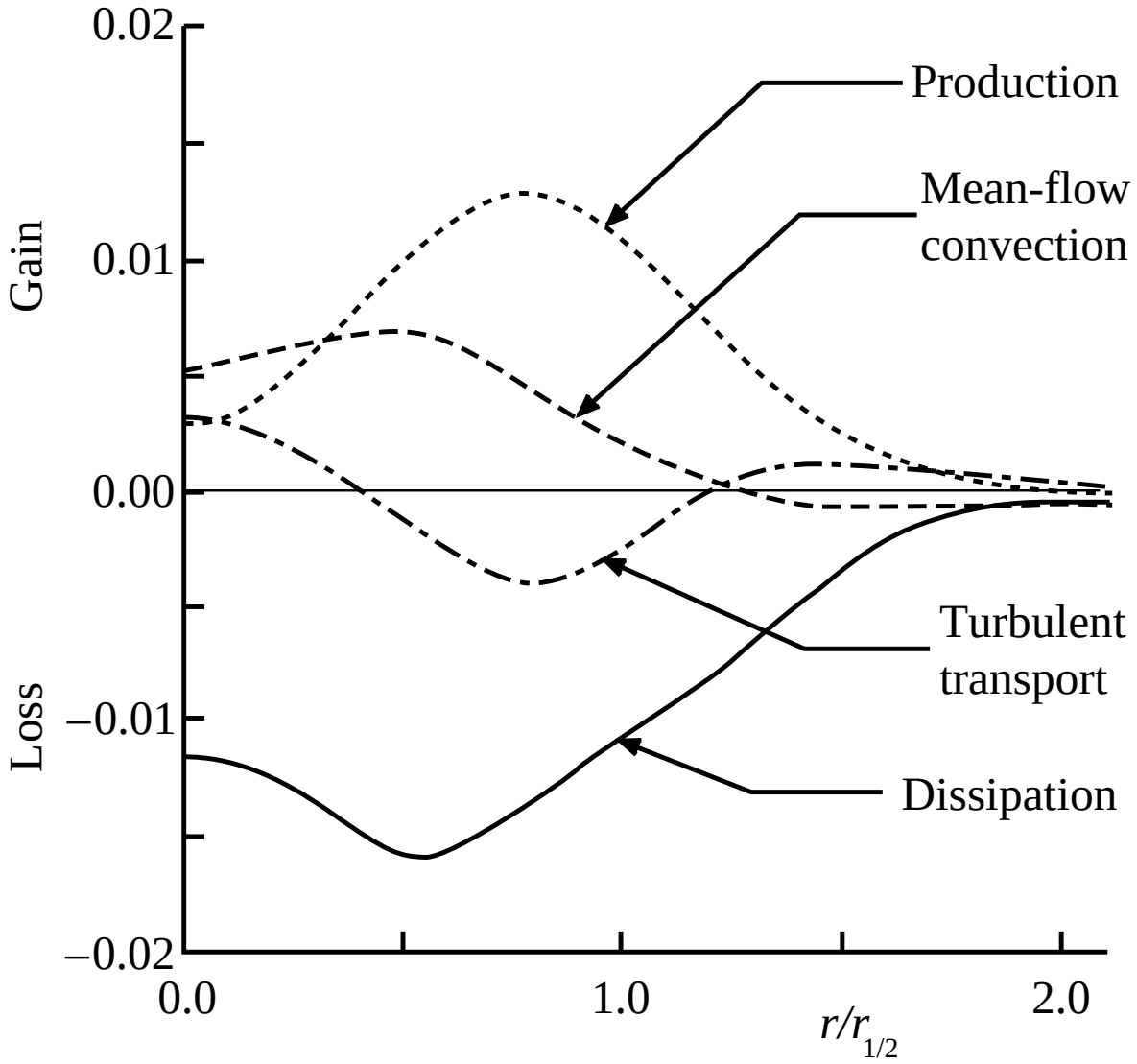

Figure 5.36: Scalar variance budget in a round jet: terms in Eq. (5.281) normalized by $\langle\phi\rangle_{y=0}, U_s$ and $r_{\frac{1}{2}}$. (From the experiment data of Panchapakesan and Lumley (1993b).)

Turbulent Flows

Stephen B. Pope
Cambridge University Press, 2000

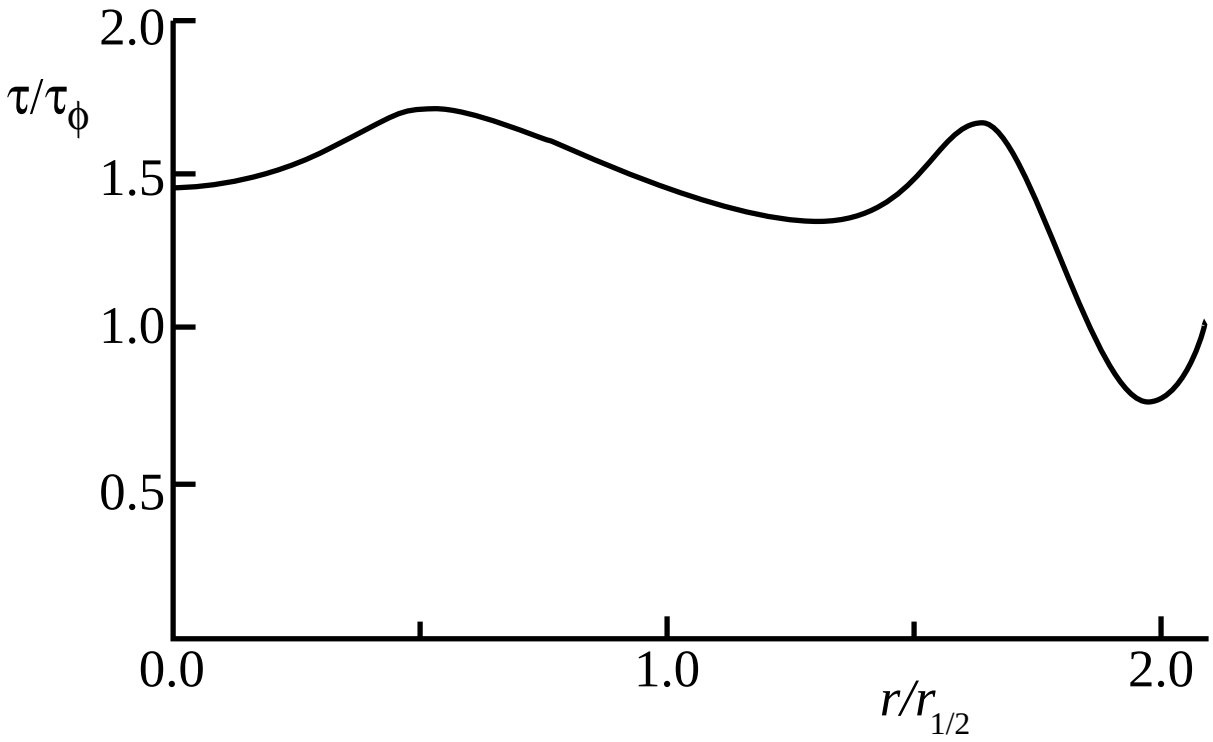

Figure 5.37: Scalar-to-velocity timescale ratio in a round jet. (From the experimental data of Panchapakesan and Lumley (1993b).)

Turbulent Flows

Stephen B. Pope
Cambridge University Press, 2000

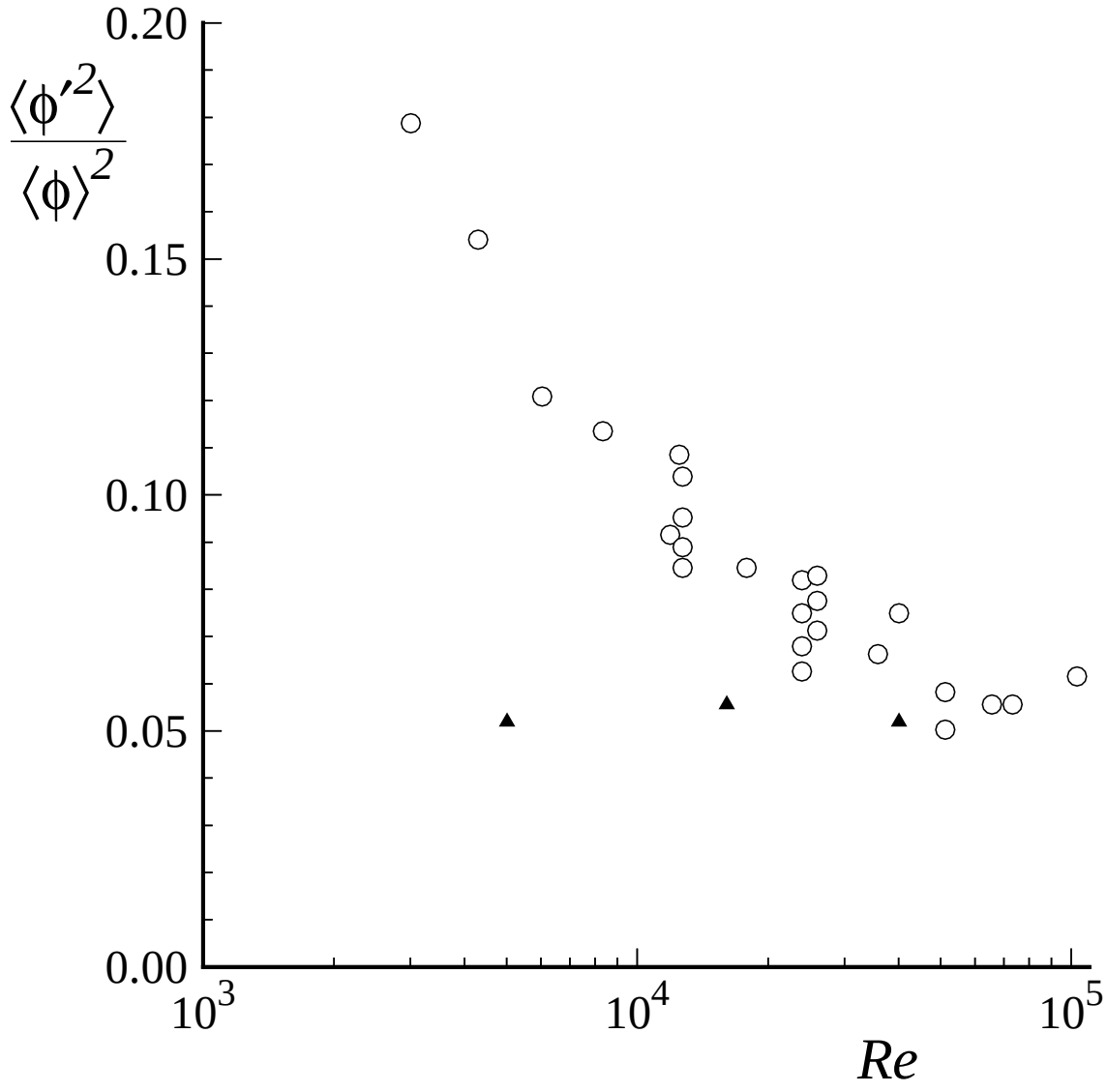

Figure 5.38: Normalized scalar variance on the axis of self-similar round jets at different Reynolds numbers. Triangles, air jets (experiments of Dowling and Dimotakis (1990); circles, water jets (experiments of Miller (1991)). (From Miller (1991).)

Turbulent Flows

Stephen B. Pope
Cambridge University Press, 2000

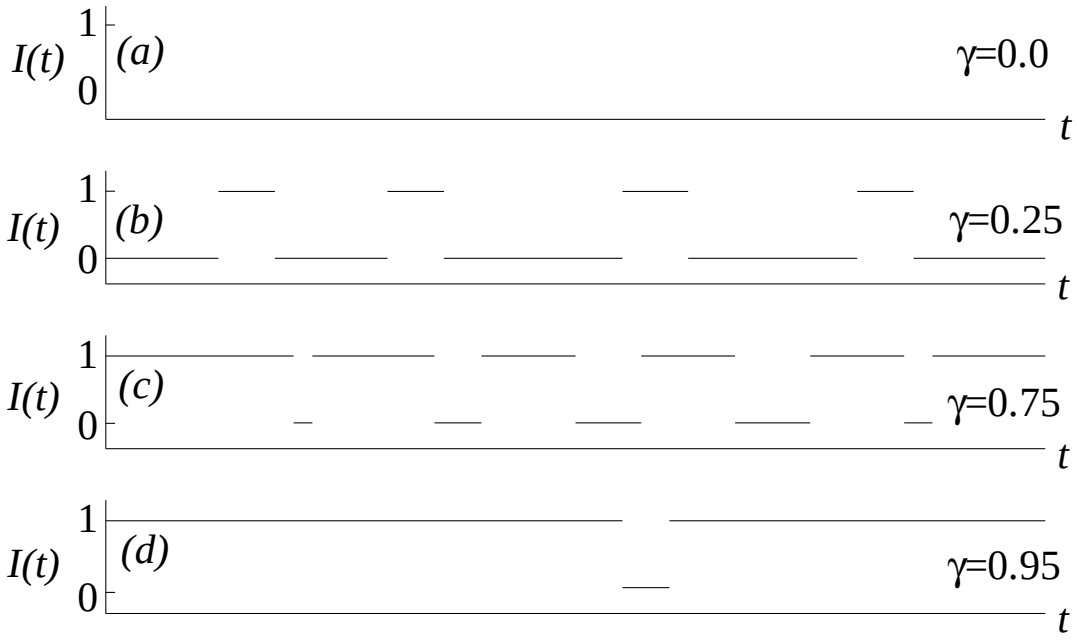

Figure 5.39: Sketch of the intermittency function vs. time in a free shear flow (a) in the irrotational non-turbulent surroundings (b) in the outer part of the intermittent region (c) in the inner part of the intermittent region and (d) close to the center of the flow.

Turbulent Flows

Stephen B. Pope
Cambridge University Press, 2000

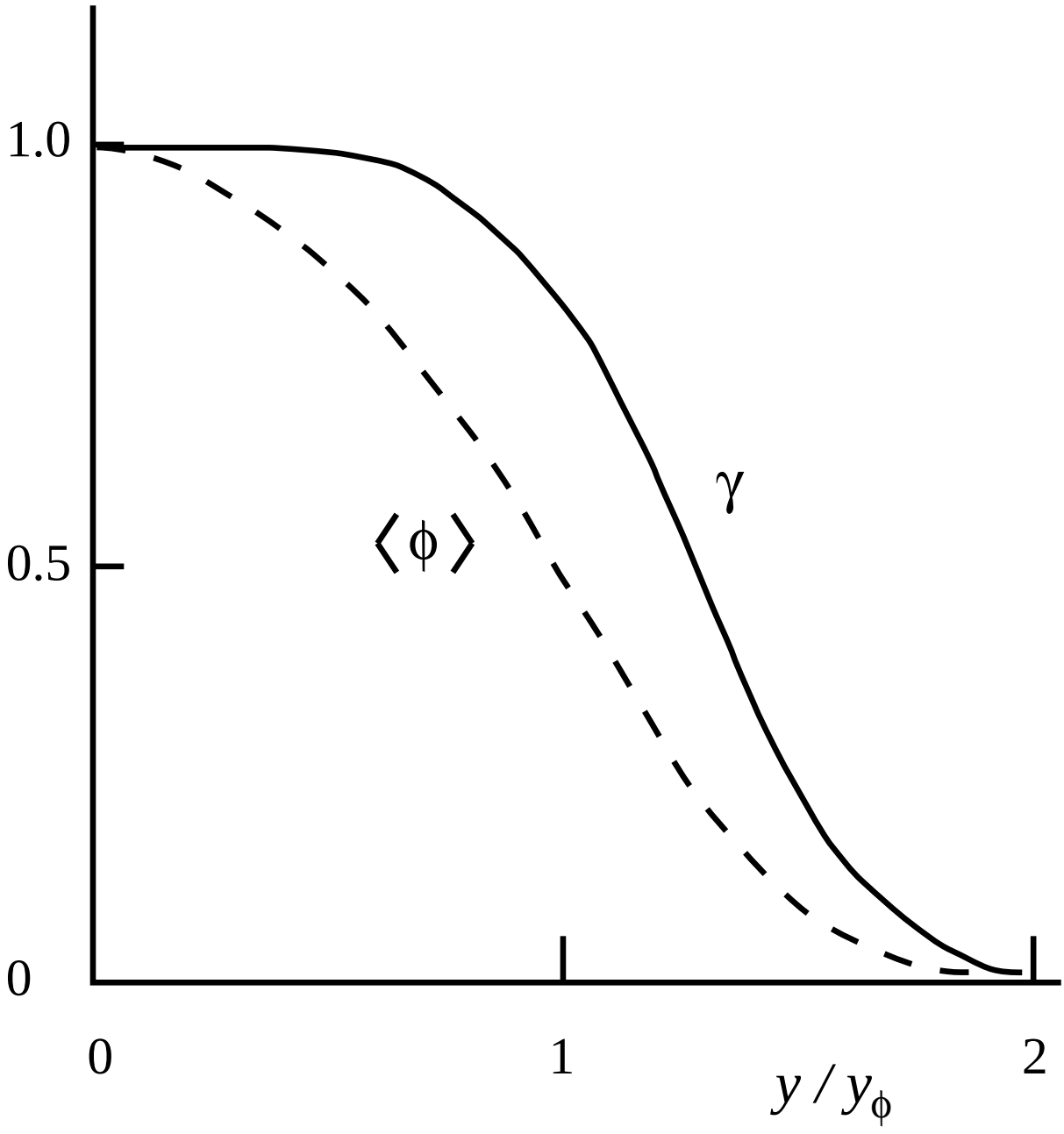

Figure 5.40: Profile of the intermittency factor in the self-similar plane wake. The mean scalar profile shown for comparison: y_ϕ is the half-width. From the experimental data of LaRue and Libby (1974, 1976).

Turbulent Flows

Stephen B. Pope
Cambridge University Press, 2000

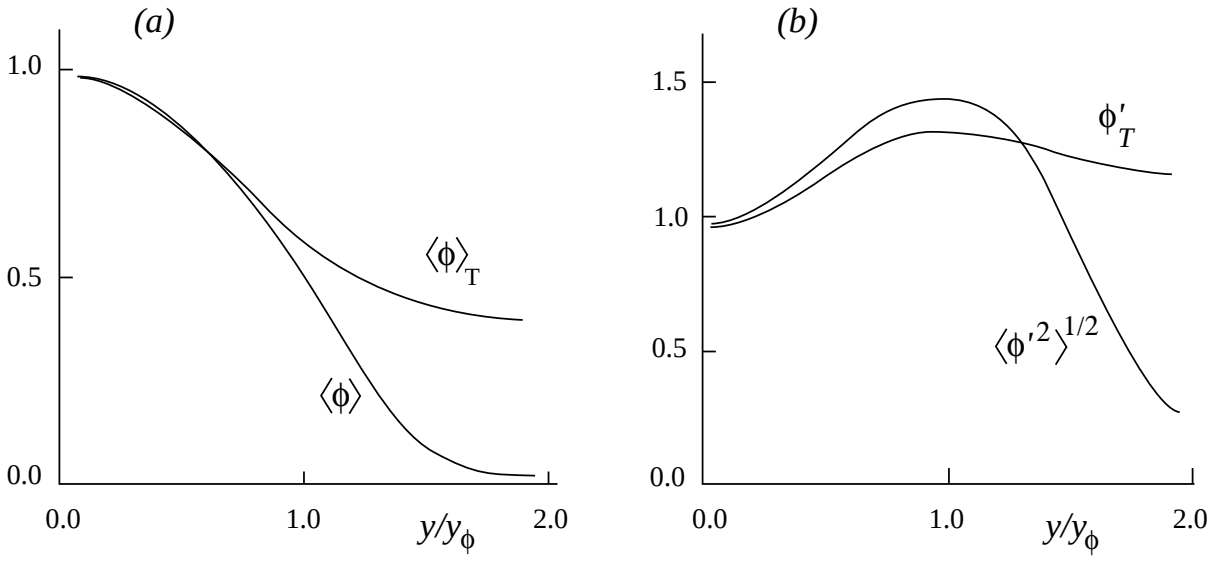

Figure 5.41: Comparison of unconditional and turbulent mean (a) and r.m.s. (b) scalar profiles in the self-similar plane wake. From the experimental data of LaRue and Libby (1974).

Turbulent Flows

Stephen B. Pope
Cambridge University Press, 2000

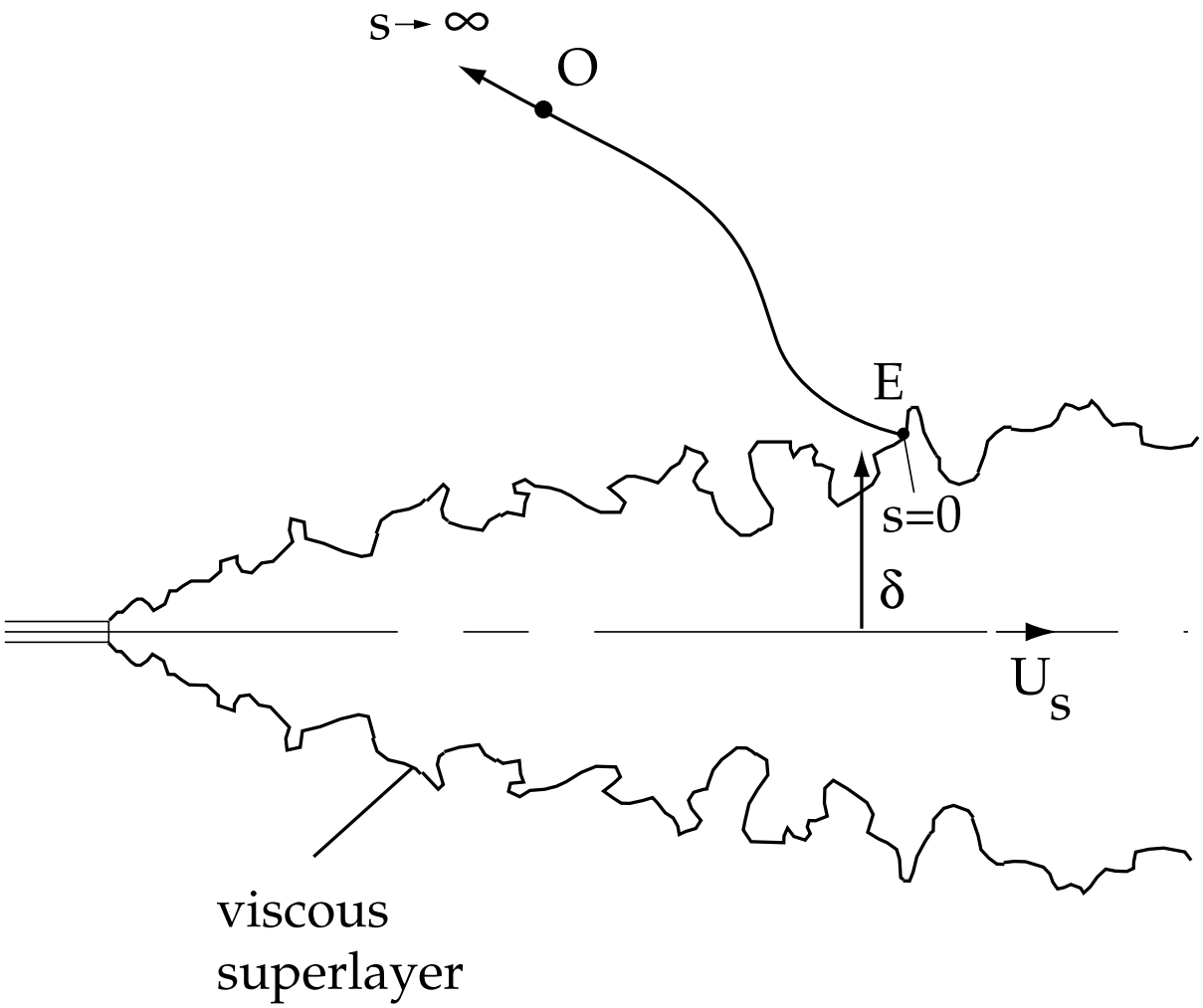

Figure 5.42: Sketch of a turbulent round jet showing the viscous superlayer, and the path of a fluid particle from a point in the quiescent ambient, O, to the superlayer, E.

Turbulent Flows

Stephen B. Pope
Cambridge University Press, 2000

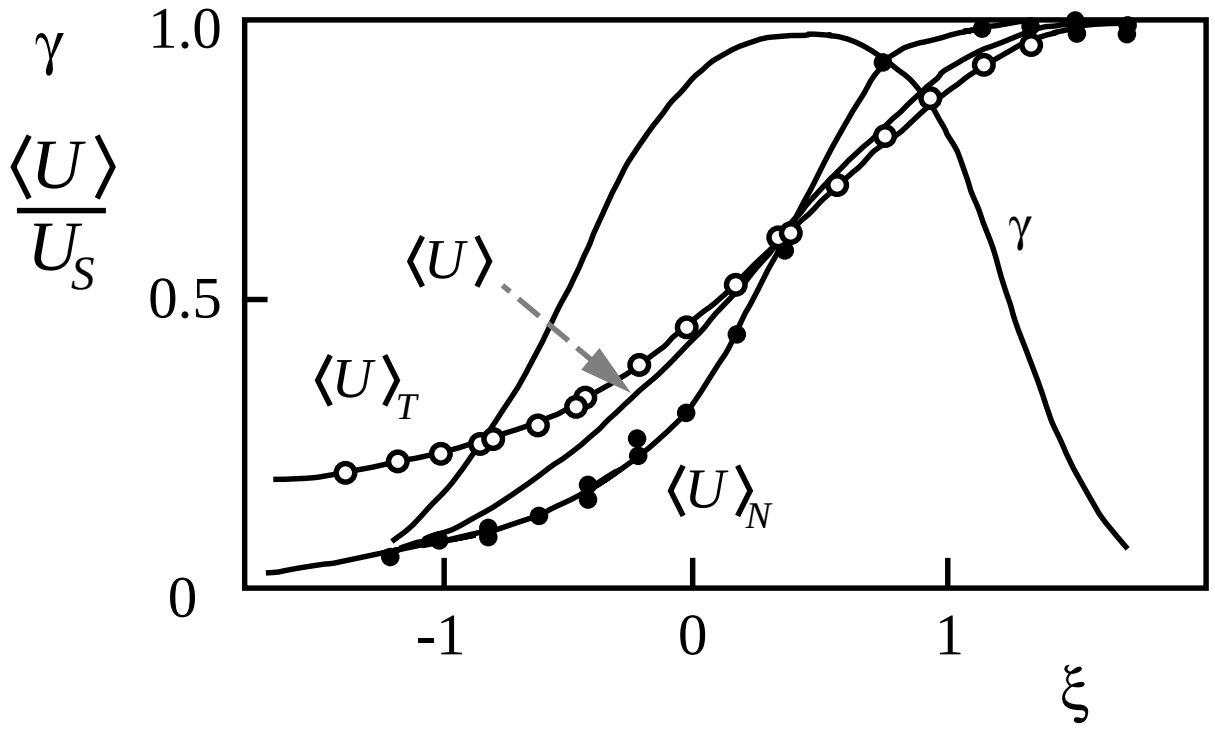

Figure 5.43: Profiles of the intermittency factor γ, the unconditional mean axial velocity $\langle U \rangle$ and the turbulent $\langle U \rangle_T$ and non-turbulent $\langle U \rangle_N$ conditional mean velocities in a self-similar mixing layer. From the experimental data of Wygnanski and Fiedler (1970).

Turbulent Flows

Stephen B. Pope
Cambridge University Press, 2000

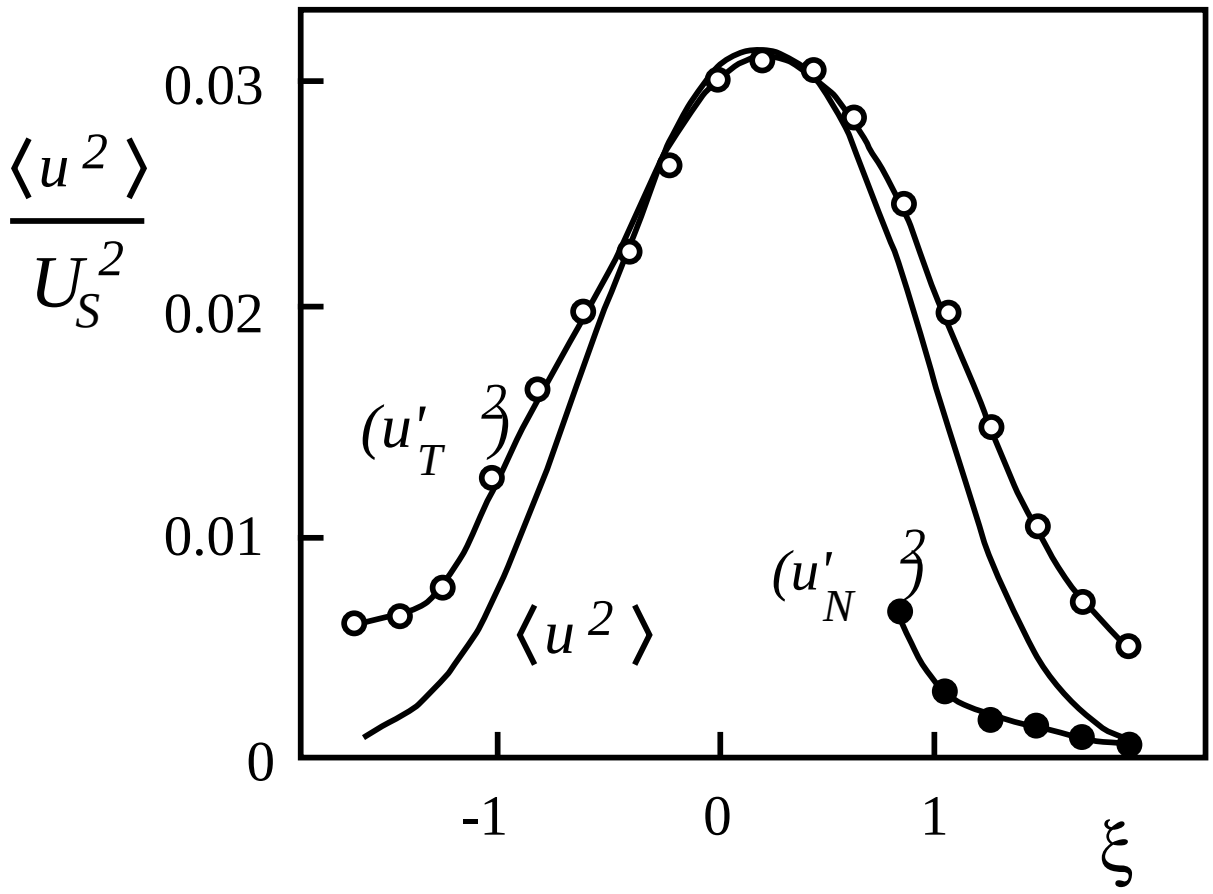

Figure 5.44: Profiles of unconditional $\langle u^2 \rangle$, turbulent $(u'_T)^2$ and non-turbulent $(u'_N)^2$ variances of axial velocity in a self-similar mixing layer. From the experimental data of Wygnanski and Fiedler (1970).

Turbulent Flows

Stephen B. Pope
Cambridge University Press, 2000

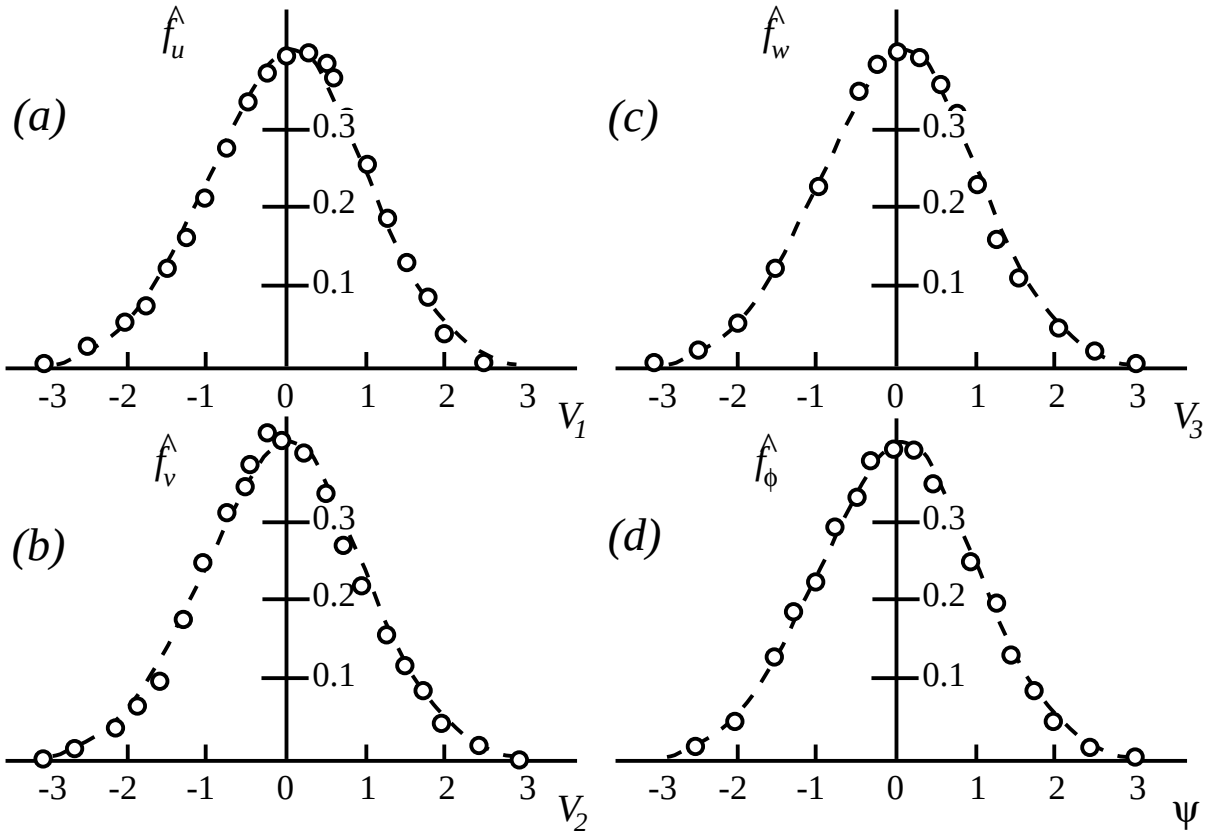

Figure 5.45: Standardized PDF's of (a) u, (b) v, (c) w and (d) ϕ in homogeneous shear flow. Dashed lines are standardized Gaussians. (From Tavoularis and Corrsin (1981).)

Turbulent Flows

Stephen B. Pope
Cambridge University Press, 2000

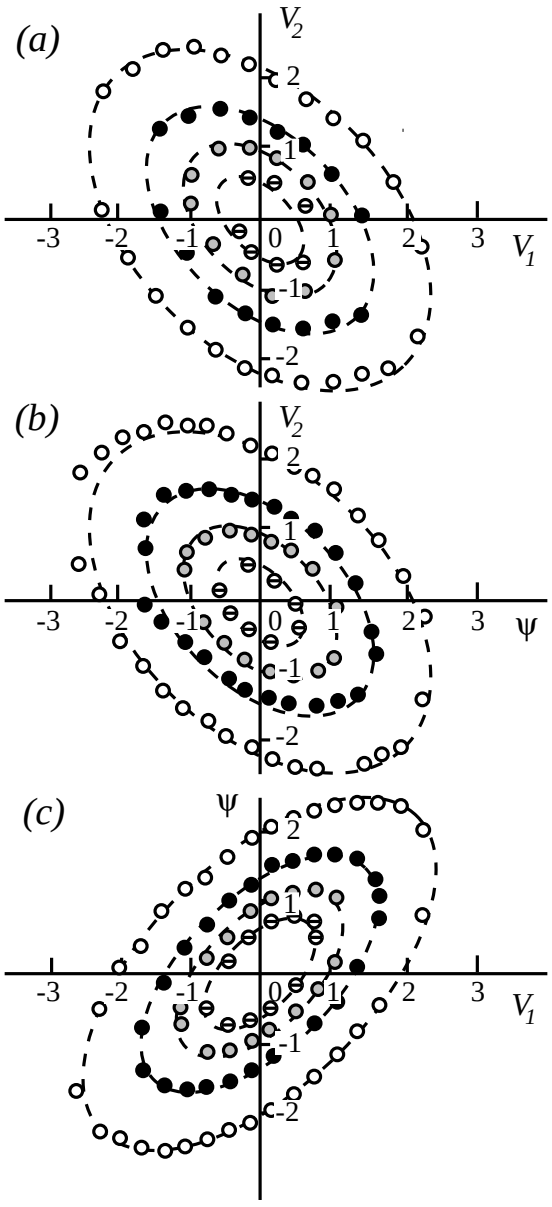

Figure 5.46: Contour plots of joint PDF's of standardized variables measured in homogeneous shear flow: (a) u and v, (b) ϕ and v, (c) u and ϕ. Contour values are $0.15, 0.10, 0.05$ and 0.01. Dashed lines are corresponding contours for joint-normal distributions with the same correlation coefficients. (From Tavoularis and Corrsin (1981).)

Turbulent Flows

Stephen B. Pope
Cambridge University Press, 2000

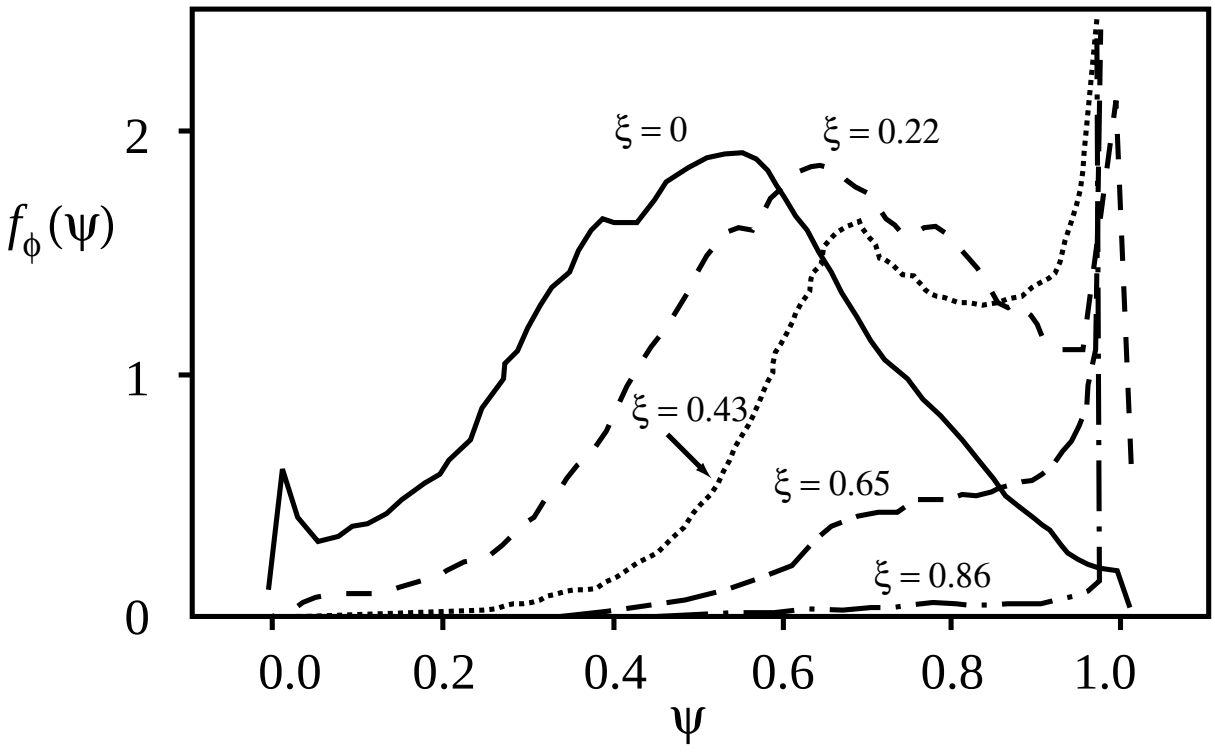

Figure 5.47: PDF's of a conserved passive scalar in the self-similar temporal mixing layer at different lateral positions. From direct numerical simulations of Rogers and Moser (1994).

Turbulent Flows

Stephen B. Pope
Cambridge University Press, 2000

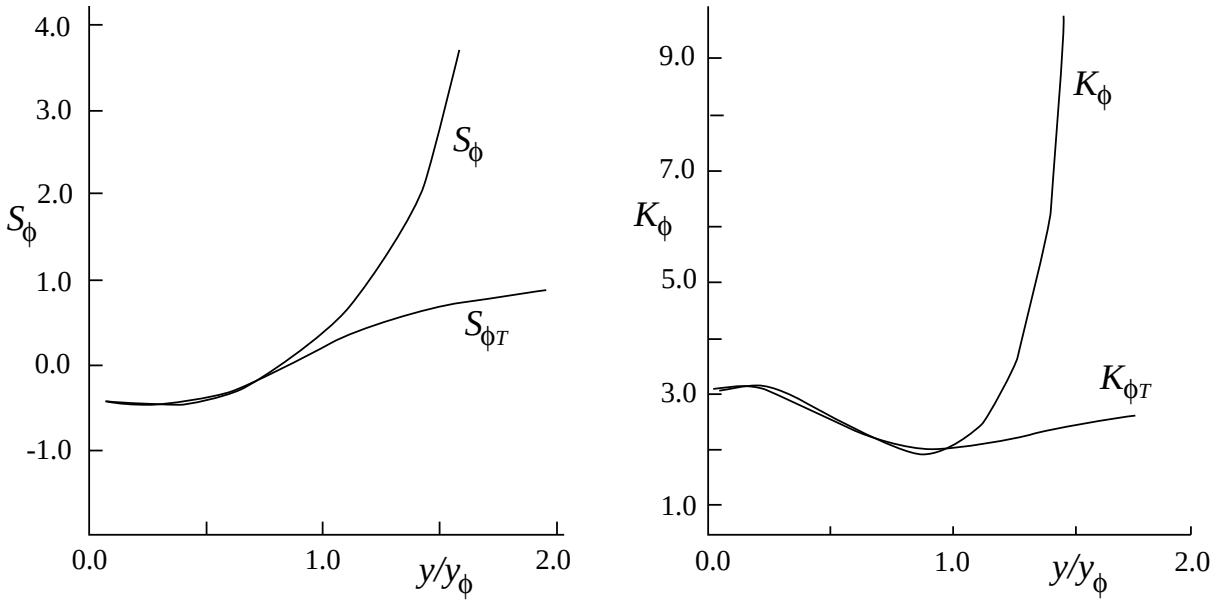

Figure 5.48: Profiles of unconditional (S_ϕ, K_ϕ) and conditional turbulent $(S_{\phi T}, K_{\phi T})$ skewness and kurtosis of a conserved passive scalar in the self-similar plane wake. From the experimental data of LaRue and Libby (1974).

Turbulent Flows

Stephen B. Pope
Cambridge University Press, 2000

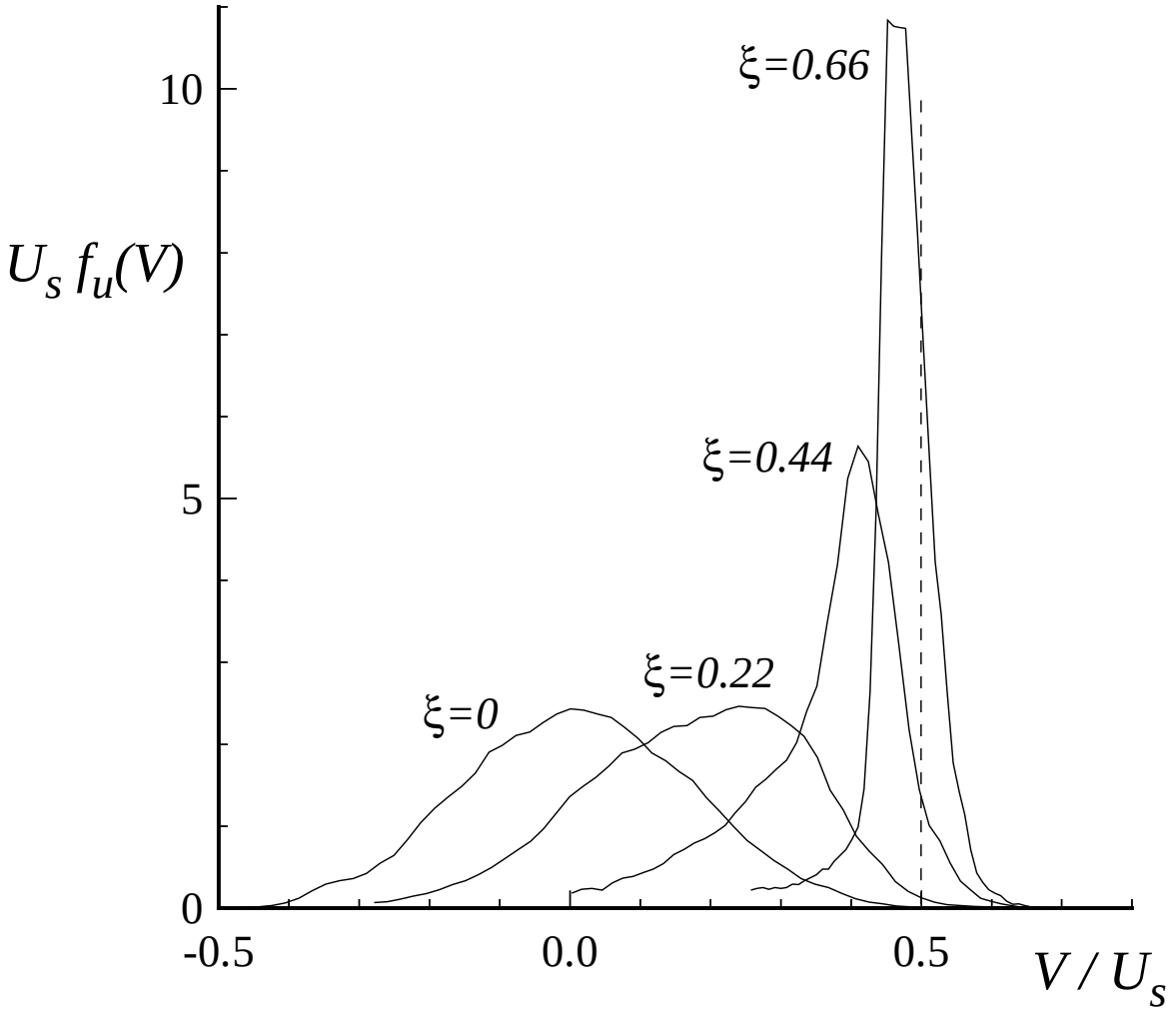

Figure 5.49: PDF's of axial velocity in a temporal mixing layer. The distance from the center of the layer is $\xi = y/\delta$. The dashed line corresponds to the freestream velocity U_h. From the DNS data of Rogers and Moser (1994).

Turbulent Flows

Stephen B. Pope
Cambridge University Press, 2000

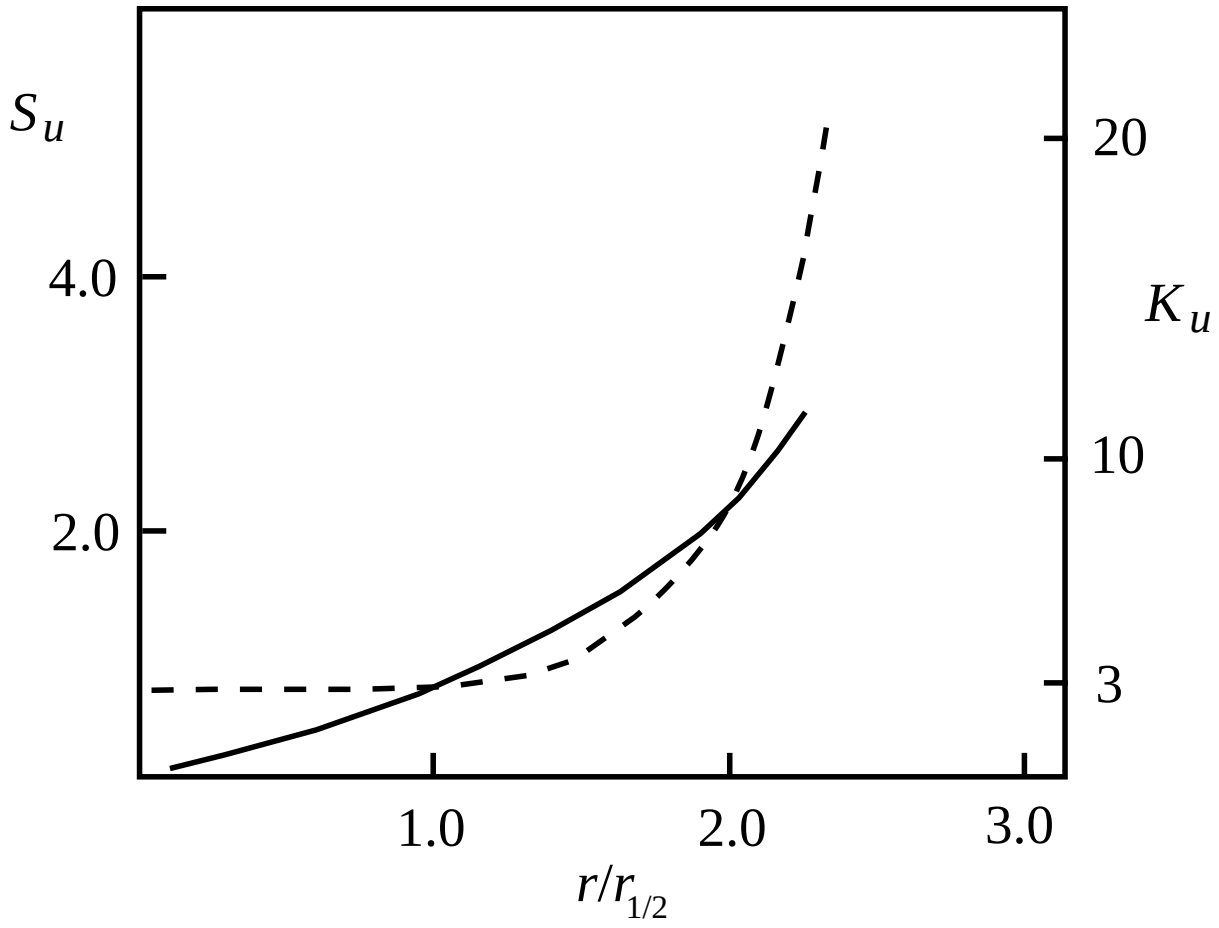

Figure 5.50: Profiles of skewness (solid line) and kurtosis (dashed line) in the self-similar round jet. From the experimental data of Wygnanski and Fiedler (1969).

CHAPTER 5: FREE SHEAR FLOWS

Turbulent Flows

Stephen B. Pope
Cambridge University Press, 2000

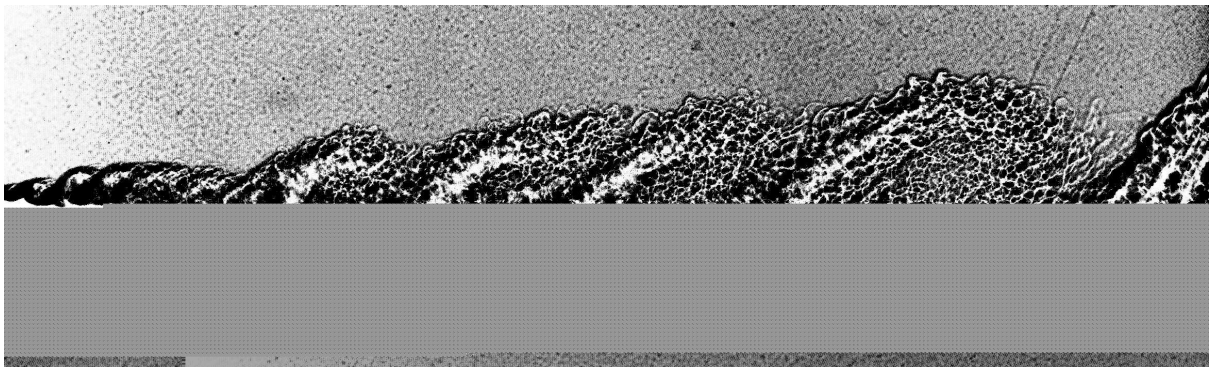

Figure 5.51: Flow visualization of a plane mixing layer. Spark shadow graph of a mixing layer between helium (upper) $U_h = 10.1 m/s$ and nitrogen (lower) $U_\ell = 3.8 m/s$ at a pressure of 8 atm. (From Brown and Roshko (1974).)

Turbulent Flows

Stephen B. Pope
Cambridge University Press, 2000

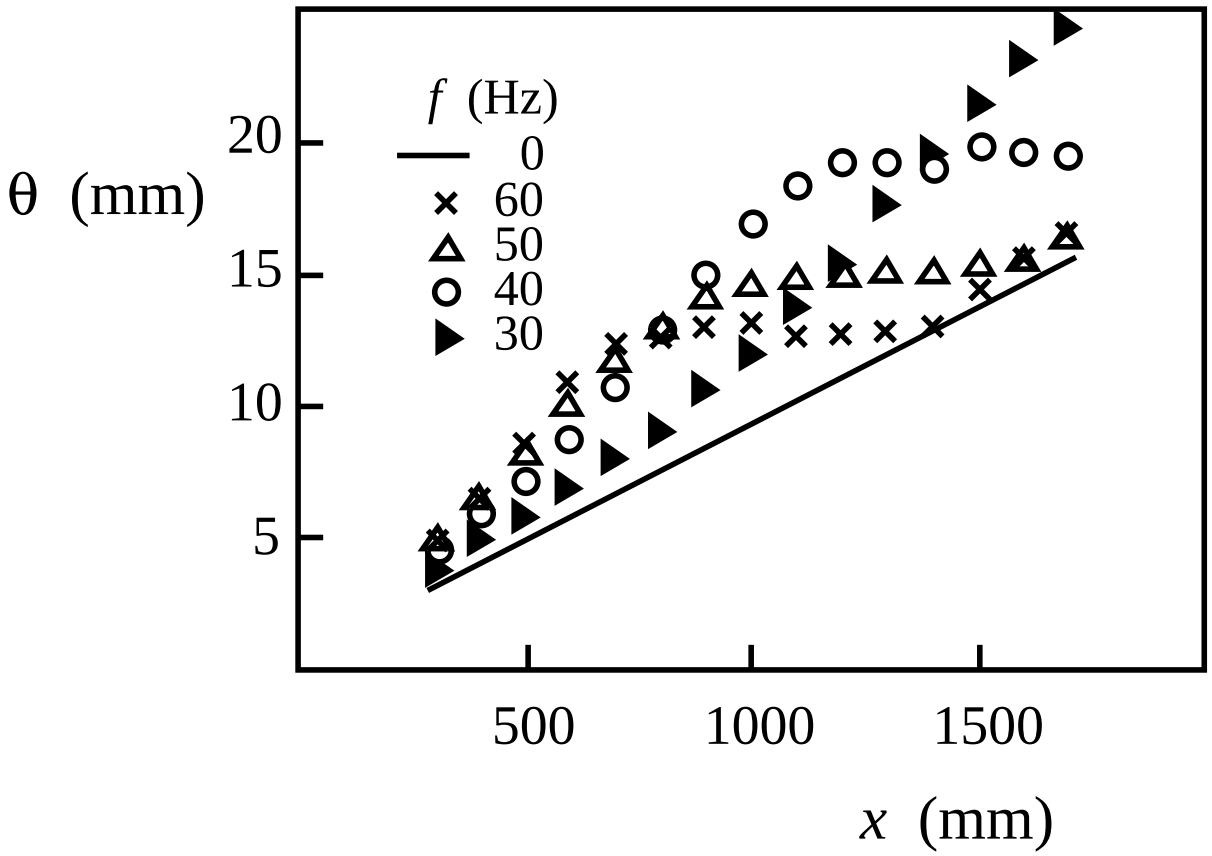

Figure 5.53: Mixing layer thickness, θ, against axial distance, x, for different forcing frequencies, f. (From Oster and Wygnanski (1982).)